Copyright © 1988, by the author(s).
All rights reserved.

Permission to make digital or hard copies of all or part of this work for personal or classroom use is granted without fee provided that copies are not made or distributed for profit or commercial advantage and that copies bear this notice and the full citation on the first page. To copy otherwise, to republish, to post on servers or to redistribute to lists, requires prior specific permission.

PROPAGATION OF LIGHT IN PERIODIC STRUCTURES WITH MATERIAL DISPERSION: GENERAL THEORY AND APPLICATION TO THE DFB SURFACE-EMITTING LASER DIODE

by

Jean-Pierre Weber, Mutsuo Ogura, Wei Hsin,
S. C. Wang, and Shyh Wang

Memorandum No. UCB/ERL M88/63

14 October 1988

PROPAGATION OF LIGHT IN PERIODIC STRUCTURES WITH MATERIAL DISPERSION: GENERAL THEORY AND APPLICATION TO THE DFB SURFACE-EMITTING LASER DIODE

by

Jean-Pierre Weber, Mutsuo Ogura, Wei Hsin,
S. C. Wang, and Shyh Wang

Memorandum No. UCB/ERL M88/63

14 October 1988

ELECTRONICS RESEARCH LABORATORY

College of Engineering
University of California, Berkeley
94720

PROPAGATION OF LIGHT IN PERIODIC STRUCTURES WITH MATERIAL DISPERSION: GENERAL THEORY AND APPLICATION TO THE DFB SURFACE-EMITTING LASER DIODE

by

Jean-Pierre Weber, Mutsuo Ogura, Wei Hsin,
S. C. Wang, and Shyh Wang

Memorandum No. UCB/ERL M88/63

14 October 1988

ELECTRONICS RESEARCH LABORATORY

College of Engineering
University of California, Berkeley
94720

Propagation of light in periodic structures with material dispersion: General theory and application to the DFB surface-emitting laser diode

Jean-Pierre Weber
Mutsuo Ogura *
Wei Hsin
S.C. Wang **
Shyh Wang

Department of Electrical Engineering and Computer Science
and Electronics Research Laboratory
University of California, Berkeley,CA 94720

ABSTRACT

We extend the Bloch wave calculation method to the case of a periodic structure where the gain (loss) and the index of refraction depend on frequency. We establish a procedure to find the propagation constants and the reflection and transmission coefficients for the Bloch waves in the general case, which has not been treated previously. We then use the results of this analysis to construct a model for a surface-emitting laser diode (SELD)[2,3], which has a vertical distributed feedback structure. This model considers the laser as an amplifier driven by spontaneous emission to compute the emission spectrum. At the present time it is valid only below threshold. We present experimental results and compare the measured emission spectrum with the theoretical one. The reasons for the discrepancies and possible improvements to the device and to the theory are then discussed.

October 14, 1988

* Electrotechnical Laboratory (ETL), 1-1-4 Umezono, Sakura-mura Niihari-gun, Ibaraki 305, Japan.
** Lockheed Missiles & Space Company, Palo Alto Research Lab, 3251 Hanover Street, Palo Alto, CA 94304.

Propagation of light in periodic structures with material dispersion: General theory and application to the DFB surface-emitting laser diode

Jean-Pierre Weber
Mutsuo Ogura *
Wei Hsin
S.C. Wang **
Shyh Wang

Department of Electrical Engineering and Computer Science
and Electronics Research Laboratory
University of California, Berkeley,CA 94720

I. Introduction

Propagation of waves in periodic structures has been studied extensively in the past and a great number of methods has been used to solve the problem. (For a good summary and references on the subject, see the review paper by Elachi [1].) There are two main types of such structures that are of practical interest for semiconductor laser diodes (Fig.1): (a) periodic waveguides and (b) multilayers. The second case is encountered in surface-emitting laser-diodes (SELD)[2,3]. These are basically distributed feedback (DFB) semiconductor lasers, with a vertical cavity and lateral p-n junction. The first order grating is formed by alternating layers of GaAs and GaAlAs. This structure is very advantageous for optoelectronic integration, since it does not need cleavage nor backside etching to form a vertical cavity, as some other SELD's require [4].

In most of the previous studies, the material characteristics of the periodic structures were supposed to be constant across the band of frequency of interest. This is a good approximation in usual edge-emitting distributed feedback (DFB) or distributed Bragg

---

* Electrotechnical Laboratory (ETL), 1-1-4 Umezono, Sakura-mura Niihari-gun, Ibaraki 305, Japan.

** Lockheed Missiles & Space Company, Palo Alto Research Lab, 3251 Hanover Street, Palo Alto, CA 94304.

reflector (DBR) laser-diodes, where we are looking at bands that are 2 to 3 nm wide. However, for SELD's, because of the strong coupling coefficients required, the stop-band has a width of 35 nm or more (in the wavelength region of 850 to 900 nm). When we have such a large bandwidth, material dispersion cannot be neglected anymore. The index of refraction can change appreciably, but the main effect is gain and loss variations with frequency in the semiconductor material. Also, because we have a multilayer where only the GaAs is pumped, we have a simultaneous index and gain grating.

In this paper, we first give a summary of the modified eigenmode theory that takes these effects into account. We also consider briefly what happens when the periodic structure does not have an even symmetry anymore. (Most of the previous studies considered structures with even symmetry only.) Then, we check the results of eigenmode theory by solving exactly the two layers case. Next, we derive the reflection and transmission coefficients for the interface between a periodic waveguide and a uniform waveguide. Using these results, we are able to compute the total reflectivity of the DFB structure used to fabricate the SELD, as a function of wavelength and we compare this result with the measured reflectivity. We then summarize the experimental data of the fabricated device. Next, we compute the theoretical emission spectrum (below threshold) and compare it to the measured emission spectrum. The model used for this calculation considers the laser as an amplifier driven by spontaneous emission. Finally, we discuss possible improvements to the theory and to the device.

We will use an extension of the eigenmode theory for periodic structures, as first developed in [5]. A good exposition can be found in [6]. The advantage over coupled mode theory (see for example [7]) is that we are really working with independent modes, which makes, in our opinion, the boundary conditions much easier to express. (Although this has been much disputed, see [8,9].) Another advantage is that it allows us to get analytical formulas for the output spectrum of a DFB laser. This is not possible with coupled mode theory [10].

II. General Theory

The equation for the propagation of a scalar wave in a one-dimensional infinite periodic medium is:

$$\frac{d^2E(z,\lambda)}{dz^2}-[g(z,\lambda)-j\beta(z,\lambda)]^2 E(z,\lambda)=0 \qquad (1)$$

where $E(z,t,\lambda)=E(z,\lambda)e^{j\omega t}$ is an electric field component ($\omega=2\pi\frac{c}{\lambda}$), $g(z,\lambda)$ is the gain (loss) constant and $\beta(z,\lambda)$ is the propagation constant. Both g and β are periodic in z and depend on λ (the free space wavelength). (The dependence on λ will not always be explicit in the rest of this paper.) The usual assumption is that $(g-j\beta)$ is an even periodic function of z. Most of the review paper by Elachi [1] treats this case. Here, we will only assume that g and β are periodic with the same period Λ, i.e., that we can write:

$$g(z,\lambda)-j\beta(z,\lambda)=g_0(\lambda)-j\beta_0(\lambda)+\sum_{\substack{q=-\infty \\ q\neq 0}}^{q=+\infty}(g_q(\lambda)-j\beta_q(\lambda))\exp(j2q\frac{\pi}{\Lambda}z) \qquad (2)$$

(where g_q and β_q are complex in general).

It is well known that the solutions of (1) are of the Floquet-Bloch type [11]:

$$E(z)=A(z)\,e^{\Gamma z}+B(z)\,e^{-\Gamma z} \qquad (3)$$

where A(z) and B(z) are periodic functions of z and Γ is the propagation constant, which is written as:

$$\Gamma=G-jK \qquad (4)$$

where G is the effective gain and K is the effective propagation constant. The usual interpretation of (3) is to say that A(z) corresponds to a forward propagating mode and B(z) corresponds to a backward propagating mode. We shall see below when this interpretation is correct. When the Bragg condition is nearly satisfied (i.e., β_0 close to K_B), the waves reflected at each interface add constructively and the reflectivity becomes high. In a passive medium, this gives a band of frequency in which Γ has a big negative

real part (as we will see below), which means that there is no propagation in that band. Hence the name stop-band is used, which is similar to the forbidden band in semiconductors. The Bragg condition at normal incidence gives for K_B:

$$\beta_0 \approx K_B = p\frac{\pi}{\Lambda} \tag{5}$$

Since the band around K_B is the one we are interested in, we will look at A(z) and B(z) in that band. Because A(z) and B(z) correspond to independent solutions of (1), we can treat them separately.

We start by expanding A(z) and B(z) in Fourier series (which we can do since they are periodic):

$$A(z,\lambda) = A_0 + \sum_{\substack{q=-\infty \\ q\neq 0}}^{q=+\infty} A_q(\lambda)\exp(j2q\frac{\pi}{\Lambda}z) \tag{6.a}$$

$$B(z,\lambda) = B_0 + \sum_{\substack{q=-\infty \\ q\neq 0}}^{q=+\infty} B_q(\lambda)\exp(j2q\frac{\pi}{\Lambda}z) \tag{6.b}$$

Then we substitute (2), (3) and (6) in (1) and by neglecting second order terms and equating terms having the same exponential factor , we get after some approximations [6]:

$$A_{+p}(\lambda) = \frac{j\kappa_+}{G+g_0+j(\delta+\delta_{eff})}A_0 = s_+(\lambda)\,A_0 \tag{7}$$

$$B_{-p}(\lambda) = \frac{j\kappa_-}{G+g_0+j(\delta+\delta_{eff})}B_0 = s_-(\lambda)\,B_0 \tag{8}$$

where:

$$\delta = K_B - \beta_0(\lambda) \qquad \delta_{eff} = K_B - K$$

$$\kappa_+ = \beta_{+p} + j\,g_{+p} \qquad \kappa_- = \beta_{-p} + j\,g_{-p} \tag{9}$$

(In equations (7), (8), (9) and in the following, p is a positive integer.) The quantities A_{+p} and B_{-p} represent Bragg-scattered waves from A_0 and B_0 respectively. Their amplitude becomes significant only when β_0 is near K_B. We can then neglect the other components,

so that (3) becomes:

$$E(z,\lambda) = A_0 [1 + s_+(\lambda) \exp(j2K_B z)] e^{\Gamma z} + B_0 [1 + s_-(\lambda) \exp(-j2K_B z)] e^{-\Gamma z} \tag{10}$$

Again, the usual interpretation is to say that the part in A_0 is a forward propagating mode and the part in B_0 is a backward propagating mode.

Let us notice that if (2) is an even function of z, we have: $\kappa_+=\kappa_-$ and $s=s_+=s_-$. In general, we have $|s_+|=|s_-|$ only if $f(z)= g(z)-j\beta(z)$ is: (1) an even function of z ($\kappa_+= \kappa_-$), (2) an odd function of z ($\kappa_+=-\kappa_-$), or (3) if $f(z)= (g_0-j\beta_0) +(g'-j\beta')h(z)$, with h(z) a real periodic function of z. This last case gives: $\kappa_+= (g'-j\beta')c_p$ and $\kappa_-= (g'-j\beta')c_p^*$ (where c_p is the pth Fourier coefficient of h(z) and c_p^* indicates the complex conjugate of c_p), i.e.: $|\kappa_+|= |\kappa_-|$. The last case includes pure index modulation ($g'=0$) and pure gain modulation ($\beta'=0$). We will have $|\kappa_+|\neq|\kappa_-|$ (and thus $|s_+|\neq|s_-|$) only if g(z) and $\beta(z)$ have different "profiles", i.e., if $f(z)= (g_0-j\beta_0)+ [g'h(z)-j\beta'p(z)]$ and p(z) is not proportional to h(z) (both are real functions).

Looking at the scattering of A_{+p} and B_{-p} into A_0 and B_0, respectively, by the same method as for (7) and (8), we get :

$$A_0 = \frac{-j\kappa_-}{(G-g_0)+j(\delta_{eff}-\delta)} A_{+p} = \frac{1}{s_+} A_{+p} \tag{11}$$

$$B_0 = \frac{-j\kappa_+}{(G-g_0)+j(\delta_{eff}-\delta)} B_{-p} = \frac{1}{s_-} B_{-p} \tag{12}$$

Substituting (7) into (11), or (8) into (12), we can now obtain the characteristic equation (which also defines P):

$$P^2 = (G+j\delta_{eff})^2 = (g_0+j\delta)^2 + \kappa_+\kappa_- \tag{13}$$

So that, by using (9) and (13) in (4):

$$\Gamma = G+j\delta_{eff}-jK_B = P-jK_B \tag{14}$$

The solutions of equation (13) in the case of even functions ($\kappa_+=\kappa_-$) are discussed for example in [1],[6] and [8]. However, all these analysis assume either a pure index modulation or a pure gain modulation and no material dispersion (i.e., the refractive index and the gain are independent of frequency). This assumption is usually valid because conventional edge-emitting DFB laser-diodes have stop-bands that are 2 to 3 nm wide, so that index and gain (loss) variations can be neglected. But in the case of our DFB-SELD structure [3], the stop-band is of the order of 35 nm and gain variations cannot be neglected anymore, especially when the gain changes from negative to positive in the stop-band, as we will see below. Also, in the case of our SELD, we have index and gain modulation at the same time (since it is formed by alternating layers of GaAs and GaAlAs and gain exists only in the GaAs; see reference [2] for details).

Looking at (13), one question comes up: Which root do we choose for P? One of these roots corresponds to the correct assignement of the forward propagating mode to A(z) and the other root makes A(z) the backward propagating mode. This is an important question since the proper definition of the reflection and transmission coefficients depends on the correct assignement of forward and backward propagation to the modes. In the previous analysis [6,8], P was chosen such that G had the same sign as g_0, or, equivalently, such that δ_{eff} had the same sign as δ. But this doesn't work in the general case and we have to find another way to decide which root defines the forward propagating mode as:

$$E(z)=A_0\,(1+s_+\exp(j2K_Bz))\,e^{\Gamma z} \tag{15}$$

Intuitively, we see that in the stop band $K \approx K_B$ (and $\delta_{eff} \approx 0$), so that the direction of the net power flow can be found by comparing the intensities of the two components (incident and backscattered) in each mode. Looking at (15), it is obvious that the direction is reversed when $|s_+|$ becomes greater than one.

More rigourously, if (15) is the only non-zero electric field component, dividing the average power flow per unit area by the average energy density, we obtain the energy velocity [6]:

$$v_E = \frac{c}{\beta_0} \frac{K - |s_+|^2(2K_B - K)}{1 + |s_+|^2} \tag{16}$$

where $\beta_0 = \bar{n}\omega\sqrt{\mu_0\varepsilon_0}$, $\bar{n}$ being the average effective index and c is the speed of light. So, if (15) really represents a forward wave, v_E has to be positive. From (16), we get then the condition:

$$\frac{1+|s_+|^2}{2|s_+|^2} \geq \frac{K_B}{K} = \frac{K_B}{K_B - \delta_{eff}} \approx 1 + \frac{\delta_{eff}}{K_B} \approx 1 \tag{17}$$

since in general $\delta_{eff} \ll K_B$. And this gives us:

$$|s_+| \leq 1 \tag{18.a}$$

And similarly, for the term in B_0 to be the backward propagating wave, we need to have:

$$|s_-| \leq 1 \tag{18.b}$$

If we consider only the cases when $|s_+| = |s_-|$, there is no contradiction between (18.a) and (18.b). There is then always a forward propagating mode and a backward propagating mode. But if we look at the general case, it is possible to have, for example (18.a) being satisfied while (18.b) is not satisfied. To see more clearly what happens, let us define: $P_1 = G + j\delta_{eff}$ and $P_2 = -G - j\delta_{eff}$. Then, looking at (7),(8),(11) and (12), we see that:

$$(s_+)_{P_1} = \frac{1}{(s_-)_{P_2}}$$

$$(s_-)_{P_1} = \frac{1}{(s_+)_{P_2}} \tag{19}$$

where the indices P_1 and P_2 mean that the coefficient is computed using that value for P. Thus, when $|s_+| = |s_-| = |s|$, we have:

$$|s|_{P_1} = \frac{1}{|s|_{P_2}}$$

This shows that in this case, the choice of the root is unambiguous. Indeed, if P_1 gives a $|s|$ greater than one, P_2 will give $|s|$ smaller than one and vice versa. Looking at the physical interpretation of s_+ and s_- from (7) and (8), we see that (18) simply says that the scattered wave amplitude cannot be bigger than the incident wave amplitude, as we found intuitively above.

But in the general case, if $|\kappa_+|$ is different from $|\kappa_-|$, we will have $|s_+|$ different from $|s_-|$ and in a certain frequency range, we could have for example $|s_+|>1$ and $|s_-|<1$. Equations (19) then show that this would be true for both roots of (13). If this is not an effect of the approximations used, and there is no reason to believe that it is, what does this mean? From the discussion above about the direction of the energy flow, the interpretation of this result is that both mode have a net energy flow in the same direction (in this case, backward)! This does not mean that there is no energy going in the forward direction, but only that there is more energy going backwards, i.e. that the reflected wave is greater than the incident wave for one of the modes. This is possible since this is an active structure.

The simplest structure that would exhibit this behavior is a three layers periodic structure, for example: $GaAs/Ga_{1-x}Al_xAs/\ Ga_{1-y}Al_yAs$, with $x \neq y$ and current injection to have gain in the GaAs layer only. This is because in this case $g(z)$ and $\beta(z)$ would have a different "profile". We applied the theory to that three layers structure and for some gain curves, we obtained the phenomenon mentioned above, i.e.: in both modes the net energy flow is in the same direction. We used these results to compute the reflectivity and transmittivity of a finite multilayer structure [12]. We then used a transmission matrix method similar to the one developed in [13] to check the reflectivity and transmittivity obtained with the eigenmode theory.The agreement of the eigenmode theory with the exact results was very good.

III. Two layers periodic structure

The case of the two layers periodic structure is interesting for several reasons. First, it is the basic structure of our surface-emitting laser-diode (SELD) [2,3], which we will analyze below. It is also a very common case in applications such as dielectric mirrors. Second, we can get exact analytical solutions without too much difficulty and this will allow us to compare them with those of the approximate theory of section II (which we will call eigenmode theory).

The structure used for the calculation is shown in figure 2. The gain and propagation constants in one period are given by:

$$g(z,\lambda)-j\beta(z,\lambda)=\begin{cases} g_1(\lambda)-j\beta_1(\lambda)=\Gamma_1(\lambda) & \text{if } -z_1<z<0 \\ g_2(\lambda)-j\beta_2(\lambda)=\Gamma_2(\lambda) & \text{if } 0<z<z_2 \end{cases} \tag{20}$$

and $z_1+z_2=\Lambda$, the period of the structure. Let us notice that if we put the origin at $z=-\frac{z_1}{2}$, the function $(g(z)-j\beta(z))$ is even in z. However, to simplify the calculations, we will use the coordinate system of figure 2 and correct later when necessary. We will suppose that we have a plane wave propagating in the direction normal to the plane of the layers, with a linear polarization in the y direction, so that equation (1) is the equation for the y component of the electric field.

Several equivalent methods can be used to solve equation (1) in this case. We will outline the one using solutions of the Floquet-Bloch type, i.e.: we start with equation (3). (Another method is used in [14].) Since A(z) and B(z) correspond to two independent solutions, we can work with them independently of one another. We will work out the solutions for A(z), and B(z) can be obtained simply by replacing Γ by $-\Gamma$ everywhere. So, we substitute (3) in (1) and we get, for A(z):

$$\frac{\partial^2 A}{\partial z^2}+2\Gamma\frac{\partial A}{\partial z}+(\Gamma^2-(g(z)-j\beta(z))^2)A=0$$

Which gives us, with $(g(z)-j\beta(z))$ defined in (20):

$$A(z)=\begin{cases} A_{+1}\exp(\gamma_{+1}z)+A_{-1}\exp(\gamma_{-1}z) & \text{if } -z_1<z<0 \\ A_{+2}\exp(\gamma_{+2}z)+A_{-2}\exp(\gamma_{-2}z) & \text{if } 0<z<z_2 \end{cases} \tag{21}$$

where:

$$\begin{cases} \gamma_{+1}=-\Gamma+\Gamma_1 & \gamma_{+2}=-\Gamma+\Gamma_2 \\ \gamma_{-1}=-\Gamma-\Gamma_1 & \gamma_{-2}=-\Gamma-\Gamma_2 \end{cases}$$

and $A(z)$ is a periodic function of z with period $\Lambda=z_1+z_2$. Using the continuity of the tangential components of the electric and magnetic fields at $z=0$ and between $z=-z_1$ and $z=z_2$ (since $A(z)$ is periodic), we get after some algebra:

$$\begin{bmatrix} 1 & 1 \\ \Gamma_1 & -\Gamma_1 \end{bmatrix} \begin{bmatrix} A_{+1} \\ A_{-1} \end{bmatrix} = \begin{bmatrix} 1 & 1 \\ \Gamma_2 & -\Gamma_2 \end{bmatrix} \begin{bmatrix} A_{+2} \\ A_{-2} \end{bmatrix} \tag{22.a}$$

and:

$$e^{\Gamma\Lambda}\begin{bmatrix} e^{-\Gamma_1 z_1} & e^{\Gamma_1 z_1} \\ \Gamma_1 e^{-\Gamma_1 z_1} & -\Gamma_1 e^{\Gamma_1 z_1} \end{bmatrix} \begin{bmatrix} A_{+1} \\ A_{-1} \end{bmatrix} = \begin{bmatrix} e^{\Gamma_2 z_2} & e^{-\Gamma_2 z_2} \\ \Gamma_2 e^{\Gamma_2 z_2} & -\Gamma_2 e^{-\Gamma_2 z_2} \end{bmatrix} \begin{bmatrix} A_{+2} \\ A_{-2} \end{bmatrix} \tag{22.b}$$

Eliminating A_{+2} and A_{-2}, we get:

$$\begin{bmatrix} A & B \\ C & D \end{bmatrix} \begin{bmatrix} A_{+1} \\ A_{-1} \end{bmatrix} = \mu \begin{bmatrix} A_{+1} \\ A_{-1} \end{bmatrix} \tag{23}$$

where $\mu=e^{\Gamma\Lambda}$ and:

$$A=e^{\Gamma_1 z_1}\left[\frac{1}{2}\left(\frac{\Gamma_1}{\Gamma_2}+\frac{\Gamma_2}{\Gamma_1}\right)\sinh(\Gamma_2 z_2)+\cosh(\Gamma_2 z_2)\right]$$

$$B=e^{\Gamma_1 z_1}\left[\frac{1}{2}\left(\frac{\Gamma_1}{\Gamma_2}-\frac{\Gamma_2}{\Gamma_1}\right)\sinh(\Gamma_2 z_2)\right]$$

$$C=e^{-\Gamma_1 z_1}\left[\frac{1}{2}\left(\frac{\Gamma_1}{\Gamma_2}-\frac{\Gamma_2}{\Gamma_1}\right)\sinh(\Gamma_2 z_2)\right]$$

$$D=e^{-\Gamma_1 z_1}\left[-\frac{1}{2}\left(\frac{\Gamma_1}{\Gamma_2}+\frac{\Gamma_2}{\Gamma_1}\right)\sinh(\Gamma_2 z_2)+\cosh(\Gamma_2 z_2)\right]$$

Which gives for the eigenvalue μ:

$$\mu=e^{\Gamma\Lambda}=\frac{T}{2}\pm\left[(\frac{T}{2})^2-1\right]^{\frac{1}{2}} \tag{24}$$

where T is the trace of the matrix and is given by:

$$T=2\cosh(\Gamma_1z_1)\cosh(\Gamma_2z_2)+\left[\frac{\Gamma_1}{\Gamma_2}+\frac{\Gamma_2}{\Gamma_1}\right]\sinh(\Gamma_1z_1)\sinh(\Gamma_2z_2)$$

In the case of no loss and no gain, this reduces to the result obtained in [14]. Let us notice that the matrix in (23) is unimodular since AD-BC=1. This also means that the two eigenvalues μ_1 and μ_2 will be inverse of one another:

$$\mu_1=\frac{1}{\mu_2} \quad \text{and} \quad \begin{cases}\mu_1=e^{\Gamma\Lambda}\\ \mu_2=e^{-\Gamma\Lambda}\end{cases} \tag{25}$$

We can check that (24) satisfies this condition. This relation was expected for symmetry reasons: One eigenvalue corresponds to the forward mode and the other one to the backward mode. But here again, we have the same problem as we had for the approximate solution: Which one is the forward mode and which one is the backward mode? Since we have only $e^{\Gamma\Lambda}$, Γ is determined only up to a term of the form $(j2m\frac{\pi}{\Lambda})$ (where m is an integer). This means that $(\Gamma\pm j2m\frac{\pi}{\Lambda})$ is also a solution of (25), for all m. The two possible solutions for a forward wave are obtained by choosing m such that the wave vector has a value close to K_B. We get then:

$$\Gamma=G+j\delta_{eff}-jK_B \quad \text{from } \mu_1 \tag{26.a}$$

$$\Gamma=-G-j\delta_{eff}-jK_B \quad \text{from } \mu_2 \tag{26.b}$$

And we use the same notation as in section II. We see that this is totally equivalent to the choice of the root of equation (13).

Hence, we will use the same criterion as in section II: the direction of the net power flow. To do that, we first have to compute the eigenvectors corresponding to the eigenvalues. We start by rewriting (21) as:

$$A(z)=\begin{cases} A_{+1}\left(\exp(\gamma_{+1}z)+s_1\exp(\gamma_{-1}z)\right) & \text{if } -z_1<z<0 \\ A_{+1}\left(s_3\exp(\gamma_{+2}z)+s_4\exp(\gamma_{-2}z)\right) & \text{if } 0<z<z_2 \end{cases} \quad (27)$$

Then, from (23), we get:

$$s_1=\frac{A_{-1}}{A_{+1}}=\frac{\mu-A}{B}=\frac{C}{\mu-D} \quad (28)$$

And, with (22.a):

$$s_3=\frac{A_{+2}}{A_{+1}}=\frac{1}{2\Gamma_2}(\Gamma_1+\Gamma_2+s_1(\Gamma_2-\Gamma_1))$$

$$s_4=\frac{A_{-2}}{A_{+1}}=\frac{1}{2\Gamma_2}(\Gamma_1-\Gamma_2+s_1(\Gamma_2+\Gamma_1)) \quad (29)$$

Notice that if we define: $s_2=\frac{A_{-2}}{A_{+2}}=\frac{s_4}{s_3}$, we get:

$$s_2=\frac{s_1+a}{1+a\,s_1} \quad \text{with:} \quad a=\frac{\Gamma_2-\Gamma_1}{\Gamma_2+\Gamma_1}$$

This is a bilinear transformation in the complex plane, and if $a\neq 0$ (i.e.: $\Gamma_1\neq\Gamma_2$), it maps the disk $|s_1|<1$ onto another disk, but with a part that has $|s_2|>1$. We can thus not rely on s_1 or s_2 alone to get the direction of the power flow, in the way we looked at s in section II.

To find the direction of the power flow, we will look at the Poynting vector's direction. But, because we have gain and/or loss in the structure, the Poynting vector is not constant along z. Therefore, we will take an average over one spatial period (of the time averaged vector):

$$\langle\vec{S}\rangle=\frac{1}{\Lambda}\int_{-z_1}^{z_2}\frac{1}{2}\mathrm{Re}(\vec{E}\times\vec{H}^*)dz \quad (30)$$

where we take: $E_y=A(z)\exp(\Gamma z)$ and $A(z)$ is defined in (27). An explicit formula is derived in Appendix A and it shows that the only non-zero component of the Poynting vector is $\langle S_z\rangle$. The sign of $\langle S_z\rangle$ will then give us the direction of the power flow: positive means forward propagation and negative means backward propagation.

Another way to find the direction of the power flow is to find the s coefficient defined in section II. To find s, we compute the first two coefficients of the Fourier series expansion of A(z) and get s as their ratio. We can then look at |s| as in section II. However, we have to be careful about one thing: the point of even symmetry is at $z=-\frac{z_1}{2}$ and that is where we have to put the origin when we compute s. If we do not do that, we will have a phase difference between the s coefficient computed here and the one defined in section II. Also, we would not have $s_+=s_-=s$. Taking that into account, we get :

$$s=e^{-jK_Bz_1}\left[\int_{-z_1}^{z_2} A'(z)\,dz \Big/ \int_{-z_1}^{z_2} A(z)\,dz\right] \tag{31}$$

where the exponential factor is due to the change of origin, A(z) is given by (27) and A′(z) also, but with the $\gamma_{\pm i}$ replaced by $\gamma_{\pm i}'$ (i=1,2):

$$\gamma_{\pm i}'=\gamma_{\pm i}-j2K_B$$

Explicitely:

$$\int_{-z_1}^{z_2} A(z)\,dz=\frac{1-e^{-\gamma_{+1}z_1}}{\gamma_{+1}}+s_1\frac{1-e^{-\gamma_{-1}z_1}}{\gamma_{-1}}+s_3\frac{e^{\gamma_{+2}z_2}-1}{\gamma_{+2}}+s_4\frac{e^{\gamma_{-2}z_2}-1}{\gamma_{-2}} \tag{32}$$

And the same for A′(z), but with the $\gamma_{\pm i}'$.

A comparison of the results obtained with |s|<1 and with the average of the Poynting vector on the examples of the next section shows only negligible differences.

IV. Examples and discussion

To illustrate the theory outlined above, we will use the two-layer structure of our surface-emitting laser-diode [2]. The layer structure is shown in figure 2 and the parameters are given in table 1. Basically, we have alternating layers of GaAs and $Ga_{0.7}Al_{0.3}As$. The thickness of each layer is chosen to be $\lambda_0/4n_i$, where λ_0 is the wavelength at which we want maximum reflectivity and n_i is the index of refraction of the layer (at λ_0). The

GaAs layer will be layer number 1 and the GaAlAs layer will be layer number 2. The loss in the GaAlAs layer is taken as independent of frequency and equal to 10 cm^{-1} (intensity loss). The gain in the GaAs layer depends on the carrier density. A semi-empirical model (based on absorption curves in [15]) was developed to get analytical expressions for the gain as a function of carrier density, temperature and wavelength. Figure 3 shows typical gain curves for three different carrier densities at 300 K. These will be used later in the examples.

Notice that the coupling constant for our structure ($\kappa \approx 4500$ cm^{-1}) is two orders of magnitude larger than for edge-emitting semiconductor DFB lasers. Also, since only the GaAs layer will be pumped, we have not only a periodic variation of the index of refraction, but also of the gain constant. This structure has even symmetry and thus $s=s_+=s_-$.

Figure 4 shows the effect on G and δ_{eff} of the introduction of gain and then gain modulation in this structure. In fig. 4(a), there is no loss or gain and we see that G is zero everywhere, except in the stop-band, where it is negative (indicating total reflection, not absorption). In fig. 4(b), a constant (independent of frequency and of z) gain of 2000 cm^{-1} is introduced in the structure. And in fig. 4(c), the periodicity of the gain is taken into account (i.e.: we have gain only in the GaAs layer, but with the same average gain). We see that the effect of gain periodicity cannot be ignored.

Figure 5 shows G and δ_{eff} for different carrier densities. In this case, the gain is not constant but depends on the wavelength. The intensity gain in the GaAs layers used for these examples is shown in figure 3. These calculations were done using the approximate (eigenmode) method of section II and the exact method of section III. The results of the two methods for G and δ_{eff} are undistinguishable at the scale of this figure. The most surprising feature of these results is the sudden jump of G from a negative to a positive value when $N=1.0\times10^{18}cm^{-3}$ (fig. 5(b)). Notice that this jump occurs at the wavelength where the average gain (g_0) changes from negative to positive.

But this is not as surprising as it seems. If we look again at fig. 4(a) and 4(b), we see that when the gain is changed from negative to positive, G (in the stop-band) changes from a large negative value to a large positive value without going to zero. What happens here, in fig. 5(b), is that the gain changes sign in the stop-band and thus G changes sign also. Mathematically, $|s|$ becomes greater than one and thus we have to switch to the other solution of (24) (or equivalently of (13)), which implies a sign change of G. Figure 6 shows a plot of $|s|$ as a function of wavelength for the two possible solutions ((26.a) and (26.b)). Since $|s|>1$ means that the direction of the power flow is reversed, we see that the eigenmodes exchange their roles at the point where $|s|=1$: The mode that was propagating in the forward direction now becomes the backward propagating mode and vice-versa.

Physically, as we can see from (16), the velocity of energy propagation is very small in the stop-band ($|s|$ is close to one), because of the multiple reflections. Thus a small loss or a small gain will be amplified a lot by the multiple reflections. In fact, we have [6]:

$$G = g_0 \left[\frac{v}{v_E} \right] \tag{33}$$

where v is the velocity of light in the medium (without the periodicity) and v_E is the energy velocity defined in (16). But this jump is only a mathematical artifact due to the method used here. The rate of change of the energy density (which is equal to $g_0 v = G v_E$, see [6]) is a continuous function of wavelength. If we compute the reflectivity or transmitivity of a finite multilayer with these formulas, we get a perfectly continuous curve (as we will see below).

Figures 5 and 6 also show that for N= $0.2\times10^{18}cm^{-3}$ and N= $2.0\times10^{18}cm^{-3}$, this phenomenon does not occur. For N= $0.2\times10^{18}cm^{-3}$, the gain is always negative and we don't have any problem. For N= $2.0\times10^{18}cm^{-3}$, the sign change of the gain (g_0) occurs outside of the stop-band and we see that G changes sign also, but without any

discontinuity. Figures 6(a) and 6(c) show that, for these cases, there is no exchange of roles between the two modes.

In figure 7, we compare the real and imaginary part of s, as computed by the approximate method (eq.(7)) and by the exact method (eq.(31)). We see that the difference is small and that for N= 1.0 $\times 10^{18}$cm^{-3}, the discontinuity occurs at exactly the same wavelength. From this and the fact that that G and δ_{eff} are correct within a few percents with the approximate method, we can conclude that the approximate method is a good approximation. We are interested in the s coefficient because it will be used in the next section to compute reflection coefficients and the emission spectrum of our DFB-SELD.

V. Reflection and transmission coefficients

We saw above that for a periodic one-dimensional medium with even symmetry, a good approximation of the electric field is given by:

$$E(z)=A_0(1+s_f)e^{\Gamma z}+B_0(1+s_b)e^{-\Gamma z} \qquad (34.a)$$

where A_0 and B_0 are the amplitude coefficients for the forward and backward propagating modes respectively and:

$$\begin{aligned} s_f &= s\exp(j2K_Bz) \\ s_b &= s\exp(-j2K_Bz) \end{aligned} \qquad (34.b)$$

Γ, K_B and s have been defined in equations (4), (5) and (7), respectively.

From these definitions, we can immediately find the forward propagation factor from z_1 to z_2 (with $z_1<z_2$)[6], that is the factor D_f such that $E(z_2)=D_f\,E(z_1)$:

$$D_f=\frac{1+s\exp(j2K_Bz_2)}{1+s\exp(j2K_Bz_1)}e^{\Gamma L}=\frac{1+s_{f2}}{1+s_{f1}}e^{\Gamma L} \qquad (35.a)$$

where $L=z_2-z_1$. Similarly, for the backward propagating factor D_b (from z_2 to z_1), such that $E(z_1)=D_bE(z_2)$, we get:

$$D_b=\frac{1+s\exp(-j2K_Bz_1)}{1+s\exp(-j2K_Bz_2)}e^{\Gamma L}=\frac{1+s_{b1}}{1+s_{b2}}e^{\Gamma L} \qquad (35.b)$$

One important point when using these formulas is that the origin of the z axis has to be at a point of even symmetry. Otherwise, we would have made a mistake because the s coefficient for the forward and backward modes would have a different phase (see the definitions (7) and (8)).

A. One interface

Let us now look at what happens at the interface between a periodic region and a uniform region (Fig.8). Expression (34) for the electric field in a periodic region is only an approximation, but, as we saw above, it is a good approximation. We will thus suppose in the rest of this paper that the electric field in a periodic region is of the form given by (34). In the uniform region, the electric field will be given by:

$$E_u(z) = A'_0 e^{-j\Gamma_u(z-z_1)} + B'_0 e^{j\Gamma_u(z-z_1)} \tag{36}$$

where Γ_u is the complex propagation constant in the uniform region and A'_0 and B'_0 are the amplitudes of the forward and backward propagating modes respectively. z_1 is the position of the interface, which we can subtract from z in (36) to simplify the calculations, since, for a uniform region, the choice of the origin is arbitrary.

Figure 8 shows the meaning of the different reflection and transmission coefficients we are going to compute. To find these coefficients, we express the continuity of the tangential electric and magnetic fields at $z=z_1$ and we get:

$$\begin{aligned} (1+s_{f1})A_0 e^{\Gamma z_1} + (1+s_{b1})B_0 e^{-\Gamma z_1} &= A'_0 + B'_0 \\ (s_{f1}-1)K_B A_0 e^{\Gamma z_1} + (1-s_{b1})K_B B_0 e^{-\Gamma z_1} &= -\beta_u A'_0 + \beta_u B'_0 \end{aligned} \tag{37}$$

where the index 1 for s_f and s_B indicates that they are computed at $z=z_1$ and where we used $\Gamma \approx K_B$ (we are working near the Bragg wavelength) and $\Gamma_u \approx \beta_u$. Now, to find, for example, R_1, we have to take the ratio of the backward and forward propagating electric fields at the interface in the periodic region:

$$R_1 = \frac{E_{p,back}(z_1)}{E_{p,forw}(z_1)} = \frac{B_0(1+s_{b1})e^{-\Gamma z_1}}{A_0(1+s_{f1})e^{\Gamma z_1}} \tag{38}$$

when there is no mode incident from the right ($B'_0=0$). We solve then (37) to find B_0/A_0 and plug the result in (38). The other coefficients are found in a similar way. We get:

$$R_1=\frac{r-s_{f1}}{1-r\,s_{b1}}\frac{1+s_{b1}}{1+s_{f1}} \qquad R_2=\frac{s_{b1}-r}{1-r\,s_{b1}}$$

$$T_1=(1+r)\frac{1-s_{f1}s_{b1}}{(1-r\,s_{b1})(1+s_{f1})} \qquad T_2=(1-r)\frac{1+s_{b1}}{1-r\,s_{b1}} \tag{39}$$

where r is the reflection coefficient due to the change in propagation constant:

$$r=\frac{K_B-\beta_u}{K_B+\beta_u}=\frac{\bar{n}-n_u}{\bar{n}+n_u} \tag{40}$$

where $\bar{n}$ is the effective index of refraction in the periodic region at the Bragg wavelength ($\bar{n}=K_B/k_0$ and $k_0=2\pi/\lambda$). and n_u is the index of refraction of the uniform region at the same wavelength.

We see that in the limit of no periodicity (s going to zero), we recover the usual expressions for the reflection and transmission coefficients. And in the limit r going to zero, we get the same results as in [6]. Now, if the periodic region is on the right instead of on the left as in figure 8, we just have to exchange s_f with s_b, R_1 with R_2 and T_1 with T_2 in (39) to get the formulas for this case. If we call R_3 the new R_1 we obtain in this way, R_4 the new R_2 and so on and if we replace z_1 by z'_2, we find:

$$R_3=\frac{s'_{f2}-r'}{1-r'\,s'_{f2}} \qquad R_4=\frac{r'-s'_{b2}}{1-r'\,s'_{f2}}\frac{1+s'_{f2}}{1+s'_{b2}}$$

$$T_3=(1-r')\frac{1+s'_{f2}}{1-r'\,s'_{f2}} \qquad T_4=(1+r')\frac{1-s'_{b2}s'_{f2}}{(1-r'\,s'_{f2})(1+s'_{b2})} \tag{41}$$

B. Phase shifter

In the following, we will also need expressions for global reflection (R', R'') and transmission (T', T'') coefficients of a phase shifter. By phase shifter, we mean, in this paper, a uniform region between two periodic regions (see figure 9). The R_i's and T_i's

(i=1,2,3,4) are the coefficients given by (39) and (41). Notice that we are using two different coordinate systems. This is necessary because, as mentioned earlier, we have to put the origin at a point of even symmetry in a periodic region. But, in general, it is impossible to have the origin (or its translation by a multiple of the period Λ) at a point of even symmetry in the two periodic regions at the same time. Hence the use of z for the left region and z′ for the right region.

The propagation factor for a uniform section of lenght L_u and with propagation constant $\Gamma_u=\beta_u+j\,g_u$ is:

$$P_u=\exp(-j\Gamma_u L_u) \tag{42}$$

We will suppose here that the reflection coefficient r is equal to zero (i.e., $\bar{n}=n_u$, which is approximately the case in our laser structure). We get then, using the method of multiple reflections:

$$R'=\frac{P_u^2 s'_{f2}-s_{f1}}{1-P_u^2 s_{b1}s'_{f2}}\,\frac{1+s_{b1}}{1+s_{f1}} \tag{43.a}$$

$$T'=\frac{P_u(1-s_{f1}s_{b1})}{1-P_u^2 s_{b1}s'_{f2}}\,\frac{1+s'_{f2}}{1+s_{f1}} \tag{43.b}$$

$$R''=\frac{P_u^2 s_{b1}-s'_{b2}}{1-P_u^2 s_{b1}s'_{f2}}\,\frac{1+s'_{f2}}{1+s'_{b2}} \tag{43.c}$$

$$T''=\frac{P_u(1-s'_{f2}s'_{b2})}{1-P_u^2 s_{b1}s'_{f2}}\,\frac{1+s_{b1}}{1+s'_{b2}} \tag{43.d}$$

The prime on the s indicates that the s coefficient for the right region can be different from the one for the left region.

VI. Reflectivity

Figure 10 and table 1 show the layer structure used for our surface emitting laser diode (SELD). From the top, we have 20 pairs of layers, consisting of one GaAs layer and one GaAlAs layer (each layer is one quarter of a wavelength thick), then we have a

quarter-wavelength GaAs layer acting as phase-shifter and finally 60 more pairs of GaAs/GaAlAs above the GaAs substrate (see [2,3]). This structure was chosen because it allows lasing in the middle of the stop-band [16], and thereby avoids the degeneracy problem of usual DFB lasers. The number of pairs at the top is smaller so that most of the power output is through the surface and not in the substrate. The structure was grown by metallo-organic chemical vapor deposition (MOCVD) for the devices we will present here, but we have also several wafers grown by molecular beam epitaxy (MBE).

In this calculation, we will consider only plane waves at normal incidence, coming from the air. Figure 11 shows the model used to compute the reflectivity. L_1 is the length of the 20 pairs section, L_2 is the length of the phase shifter and L_3 is the length of the 60 pairs section. The R_i's and the T_i's we need are given by the formulas derived in the previous section and are summarized in Appendix B.

Using the method of multiple reflections, we find the total power reflectivity to be given by:

$$R_P = |R_T|^2 \tag{44.a}$$

and

$$\begin{aligned} R_T &= R_1 + \frac{T_1 T_2 R_{eff} P_1 P_2}{1 - R_2 R_{eff} P_1 P_2} \\ R_{eff} &= R_3 + \frac{T_3 T_4 R_5 P_3 P_4}{1 - R_4 R_5 P_3 P_4} \end{aligned} \tag{44.b}$$

where the P_i's are propagation factors of the type given by (35) (D_f and D_b) and R_{eff} is an effective reflection coefficient for the phase-shifter and everything that is to its right (in fig. 11). If we look at the formulas we obtained, we see that a lot of factors of the form $(1+s_f)$ or $(1+s_b)$ can be cancelled out. This can be done by omitting the factors between square brackets in Appendix B.

Before we can compute the power reflectivity of our structure, we need to define two more characteristics: the index of refraction and the absorption as functions of

wavelength. We will assume that the index of refraction is constant and that the absorption coefficient in the GaAlAs layer is constant and equal to 10 cm^{-1} (intensity coefficient). For the GaAs layer, we will use:

$$\alpha(E) = \left[\frac{1}{\beta} + \frac{1}{\gamma} \right]^{-1} \quad [cm^{-1}]$$

$$\begin{aligned} \beta &= \exp(4.85E + 1.9552) \\ \gamma &= \exp(118.84E - 159.9106) \end{aligned} \tag{45}$$

where E is the photon energy in eV. This formula was obtained by fitting to a measured absorption curve for small p-type doping given in [15].

Now we can compute the power reflectivity of our structure. Figure 12(a) gives the result of the calculation for the structure as defined by figure 10 and Table 1. In Figure 12(b), we see a typical experimental result. The measurements were made using a Perkin-Elmer Lambda 9 spectrometer with the Absolute Reflectance Accessory. In this apparatus, the beam normally reflects twice from the sample at two different positions, with an angle of 8 degrees. Because of the small size of the sample and of its non-uniformity, an aluminium mirror was substituted at the second reflection point. We did a first measurement with the sample, then replaced it with an aluminium reference mirror. This allowed us to compute the absolute reflectivity, knowing the reflectivity of the aluminium. The fact that we were not at normal incidence (but 8 degrees off) slightly increases the apparent thickness of the layers (less than 1%), but can otherwise be neglected.

We can see that the experimental result is similar to the theoretical result of fig. 12(a), but that there are some differences also. The main difference is the double dip in the middle of the stop-band for the experimental result. This can be explained by looking at what happens when the thickness of each layer changes by one lattice constant ($a \approx 5.65$ Angstroms). This gives us a change of tickness of about 0.9 %, which, for an original Bragg wavelength of 890 nm (in vacuum), corresponds to a change of about 8 nm. This

corresponds approximatively to the spacing of the two dips. What happens is that the grown structure is not uniform across the wafer and the spot size for the reflectivity measurement is several millimeters. The measured reflectivity is thus an average of two different thicknesses.

We varied the parameters slightly to try to reproduce the experimental curve. Our best result is the theoretical curve in Fig. 12(b) (but it is not an optimal fit). It was obtained by a weighted average between a Bragg wavelength (λ_0) of 889 nm (70 %) and a λ_0= 897 nm (30 %), with the thickness of the top GaAs layer (the one in contact with air) reduced to 37 nm (instead of 67 nm). (This reduction in thickness could happen during wafer processing and handling.)

We did not try to improve the agreement between theory and experiment because it depends on too many unknown parameters, such as the exact dependence of the loss on wavelength, and because the theory used here is only an approximation. We also neglected the variation of the index of refraction with wavelength. However, we get correctly the main characteristics of the curves and this gives us confidence for applying the theory to the calculation of the emission spectrum of the SELD (in section VIII).

VII. The surface-emitting laser diode

As described previously in [2] and [3], the surface emitting laser diodes (SELD) are fabricated by starting from wafers having the layer structure described above (Fig. 10 and Table 1). Mesas with dimensions ranging from 2 x 8 to 3 x 17 μm^2 at the top surface are formed by wet etching. Then a n-type $Ga_{0.6}Al_{0.4}As$ cladding layer is grown around the mesas by selective liquid phase epitaxy (LPE). Finally, a lateral pn junction is formed by selective zinc diffusion through an opening in a silicon nitride film, at a distance of 3 to 4 μm away from the edge of the mesa. Figure 13(a) shows the structure of the laser and Fig. 13(b) is a scanning electron microscope (SEM) picture of a laser. The zinc diffusion region is brigther in this picture. The total thickness of the structure is about 10 μm.

Since the GaAs/GaAlAs multilayer is completely surrounded by GaAlAs, carrier confinement in this structure should be comparable with that of buried heterostructures. Carriers are injected predominantly in the GaAs layers and therefore we will assume in the model that only the GaAs layers are pumped. There is however the possibility of current leakage around the mesa. We believe this happens at high currents.

Figure 14 shows the light output versus dc current characteristics (L-I curve) of a SELD at room temperature. We get what looks like typical threshold currents in the range from 2 to 10 mA and differential quantum efficiencies from 0.3 % to 1.36 %. Powers of 0.5 mW for a current of 50 mA have been observed for CW operation at room temperature. More recently, we obtained quantum efficiencies up to 5 % for some devices. Unfortunately, they were accidentely destroyed before their spectrum could be measured.

Observation of the near-field pattern shows [2,3] that the light-emitting region is confined within the rectangular top surface of the multilayer (at least when the current is not too high). The far-field pattern is circular [2,3] and its beam divergence angle, for a current of 20 mA, is 7 to 8 degrees. However the circular emission pattern is surprising for a device with a rectangular emission surface. The 7 to 8 degrees angle corresponds roughly to a width of about 3 μm for the rectangular opening, but the length of about 15 μm should give a much narrower beam in that direction (about 3 degrees), if it were a diffraction limited beam. Obviously, the beam is not diffraction limited in that direction. A reason for that could be that there is no coherence between points more than 3 μm apart.

Figure 15 shows the spectrum of the SELD at different currents, for CW operation at room temperature. We see that there is a sharp emission line at 884 nm which becomes obvious for a drive current of 1.6 mA. This is consistent with the L-I curve, which shows what looks like a 2 mA threshold current. The half-width is rather large (1.5 to 3 nm) compared to conventional edge-emitting laser diodes. The total width of

the emission spectrum is also large (about 50 nm), compared to edge-emitting lasers.

In view of these results, one might ask whether these devices are really lasing? We think they are. There may be several reasons for the low quantum efficiency: leakage current around the mesa, non-radiative recombination at interfacial defects if the LPE was not very good and a big spontaneous emission component. We explain below how the shape of the mesa can lead to a lot of parasitic spontaneous emission which lower the quantum efficiency and can also affect the spectrum.

VIII. Emission spectrum of the SELD

In this section, we develop a model (figure 16) to reproduce and explain the emission spectrum, at least below threshold. It is very similar to the one used to compute the reflectivity and we make the same assumptions, except that we will now have gain in the pumped section (which is taken as being the zinc diffused region). In addition, we assume that this pumped section has a uniform carrier density (in the GaAs part of the layers) and that the unpumped region is uniform and lossy. These assumptions are rough approximations, but they allow us a relatively easy calculation using what we did in the previous sections.

The reflection and transmission coefficients are given in Appendix B. E_1, E_4 and E_2, E_3 are the electric fields amplitudes of the forward and backward propagating modes respectively, at the two interfaces of the phase shifter region (L_2). E_{out} is the amplitude of the electric field of the light output. The S_i's are the equivalent sources for the electric fields at the interfaces due to the spontaneous emission in sections L_1 and L_3 (we neglect the spontaneous emission in the phase shifter).

If we express the electric fields as functions of one another and of the S_i's, we get the following system of equations:

$$\begin{aligned}
E_1 &= R_2P_1P_2E_2 + R_2P_1S_1 + S_2 \\
E_2 &= R_3E_1 + T_4E_3 \\
E_3 &= R_5P_3P_4E_4 + R_5P_4S_4 + S_3 \\
E_4 &= R_4E_3 + T_3E_1 \\
E_{out} &= T_2P_2E_2 + T_2S_1
\end{aligned} \tag{46}$$

If we eliminate the E_i's, we find:

$$E_{out}=(R_2T_2P_1P_2\frac{N}{D}+T_2)S_1+(T_2P_2\frac{N}{D})S_2+(T_2P_2\frac{T_4}{D})S_3+(R_5T_2P_2P_4\frac{T_4}{D})S_4 \quad (47)$$

where:

$$N=R_3+R_5P_3P_4(T_3T_4-R_3R_4)$$
$$D=(1-R_2R_3P_1P_2)(1-R_4R_5P_3P_4)-R_2R_5T_3T_4P_1P_2P_3P_4$$

But what we are interested in is the output power. To convert the relation (47) between the electric fields to a relation between the power in the modes, we have to remember that the S_i's are really of the form given by (34), i.e.:

$$S_i=S_{i0}(1+s\exp(\pm 2jK_Bz_i))\,e^{\pm\Gamma z_i}$$

while we have:

$$E_{air}(z)=E_0\,e^{-j\frac{2\pi}{\lambda}(z-z_1)} \quad \text{and} \quad E_{out}=E_{air}(z_1)=E_0$$

Then, with the same cancellations of factors as for the reflectivities, we get:

$$|E_{out}|^2=|R_2T_2P_1P_2\frac{N}{D}+T_2|^2\,|S_{10}|^2+|T_2P_2\frac{N}{D}|^2\,|S_{20}|^2+|T_2P_2\frac{T_4}{D}|^2\,|S_{30}|^2$$
$$+|R_5T_2P_2P_4\frac{T_4}{D}|^2\,|S_{40}|^2=\sum_{j=1}^{4}C_j\,|S_{j0}|^2 \quad (48)$$

where we have taken into account the fact that the S_i's are not coherent with one another. This formula is valid with the reflection and transmission coefficients as given in Appendix B when we omit the factors between square brackets. Now, by computing the Poynting vector for a field of the type of (34), we find a relation between the power density p_j and $|S_{j0}|^2$:

$$p_j=\frac{1}{2\omega\mu_0}[K-|s|^2(2K_B-K)]\,|S_{j0}|^2$$

And for the output power:

$$p_{out}=\frac{k_0}{2\omega\mu_0}\,|E_0|^2$$

This gives us then the ouput power spectral density:

$$p_{out}=\frac{k_0}{K-|s|^2(2K_B-K)}\left\{\sum_{j=1}^{4}C_j p_j\right\} \tag{49}$$

where the C_j's were defined in (48) and the p_i's (defined below) are the spectral power densities due to the spontaneous emission.

We see immediatly from (48) and (49) that we will have lasing when D=0. This condition will give us the wavelengths of the modes and the corresponding gain thresholds. (Do not forget that the reflection and transmission coefficients are wavelength dependent and that the propagation factors depend on the wavelength and on the gain.)

If we solve the equation D=0, we get several solutions, each one corresponding to a mode. If we use λ_0= 890 nm and a phase shifter thickness reduced to 0.4 Λ (instead of 0.5 Λ), we will see below that we get the best spectrum adjustment. This gives us a mode at 884 nm with a threshold intensity gain of about 44 cm^{-1} (for the material gain of GaAs). With the model for the gain developed below, this corresponds, at that wavelength to a threshold carrier density of about 1.6×10^{18} cm^{-3}. We can now estimate the threshold current with:

$$I_{th}=q\frac{tldN_{th}}{\tau}$$

where t= 2 μm and l= 15 μm are the mesa dimensions and d≈ 3 μm is the active layers' thickness (without the GaAlAs layers) and τ= 4 ns is the spontaneous lifetime (q is the electron charge). This gives us $I_{th}\approx 7.76$ mA, which is in the range of observed threshold currents. The other modes, which will give humps in the spectrum, have much higher threshold gains (several thousands cm^{-1} at least).

Let us now find expressions for the p_i's in terms of the spontaneous emission spectral density rate and the device parameters. To simplify the calculations, we will suppose a uniform spontaneous emission in the whole section (which is consistent with the uniform carrier density) and we correct then for the fact that we have emission only in the

GaAs layers with a factor f. This factor f is equal to the ratio of the thickness of one GaAs layer to one period. Now, to get the p_i's, we sum incoherently the amplified spontaneous emission in each section. For example, we get for p_1:

$$p_1 = f\frac{tl}{2}E\, r_{sp}(E)\,\gamma \int_0^{L_1} |e^{\Gamma z}|^2 dz$$

where γ is the fraction of the spontaneous emission coupling to the cavity mode, E is the photon energy (in Joules) and $r_{sp}(E)$ is the spontaneous emission spectral density rate per unit volume. The cavity cross-section, $t \times l$, is taken as constant. The factor one half comes from the fact that only one half of the spontaneous emission coupled to the cavity mode goes in one direction. Using equation (14), we have:

$$|e^{\Gamma z}|^2 = e^{2Gz}$$

which gives us:

$$p_1 = p_2 = f\frac{tl}{2}E\, r_{sp}(E)\,\gamma\left[\frac{e^{2GL_1}-1}{2G}\right] \tag{50.a}$$

and:

$$p_3 = p_4 = f\frac{tl}{2}E\, r_{sp}(E)\,\gamma\left[\frac{e^{2GL_3}-1}{2G}\right] \tag{50.b}$$

Putting (49) and (50) together, we find:

$$p_{out} = f\frac{tl}{2}E\, r_{sp}(E)\left[\frac{\gamma k_0}{K-|s|^2(2K_B-K)}\right]\left\{(C_1+C_2)\left[\frac{e^{2GL_1}-1}{2G}\right] + (C_3+C_4)\left[\frac{e^{2GL_3}-1}{2G}\right]\right\} \tag{51}$$

Finally, let us notice that this is $p_{out}(E)$. If we want $p_{out}(\lambda)$, since $E=hc/\lambda$, we have to use:

$$p_{out}(\lambda) = p_{out}(E)\left|\frac{dE}{d\lambda}\right| = p_{out}(E)\frac{E^2}{hc}$$

The factor between square brackets in (51) has to be examined carefully. It can be shown [17] that in a periodic waveguide, γ becomes dependent on wavelength and contains a factor that cancels the denominator. The expression between square brackets is

then equal to the γ in an uniform waveguide times a factor of order unity depending on wavelength. In this paper, we will neglect that factor, although it modifies somewhat the spectrum [17].

Now, only two factors remain to be specified before we can compute the emission spectrum. These are the spontaneous emission rate $r_{sp}(E)$ and the GaAs material gain $g_1(E)$. Both will be functions of the carrier density. For the spontaneous emission rate, we know [15] that for the non-thermal equilibrium case, we have:

$$r_{sp}(E) = \frac{1}{\pi^2 \hbar^2 v^2} \frac{-E^2 g(E,N)}{e^{(E-\Delta\varepsilon_F)/k_B T} - 1} \qquad [J^{-1} m^{-3} s^{-1}] \tag{52}$$

where v is the light's velocity in the material, E is the photon energy, k_B is Boltzmann's constant and T is the temperature. The difference between the electron and hole quasi-Fermi levels ($\Delta\varepsilon_F$) can be computed from the carrier density N by using the Fermi-Dirac distribution and the parabolic approximation for the band extrema. Using this and experimental absorption curves from [15], we developed a semi-empirical model for the gain as a function of E, N, T and N_A, where N_A is the acceptor concentration (zinc gives a p-type doping). Figure 17(a) shows typical gain curves for different carrier densities, at constant temperature, and figure 17(b) for different temperatures, at constant carrier density.

At this point, we have not yet incorporated rate equations in our model to allow us to compute the L-I characteristic. Therefore, we will postulate a carrier density and compute the shape of the emission spectrum, but we will not try to get the absolute values. Thus we do not need to worry about the constants in (50) and (51). The final result is shown in figure 18(a) and can be compared with the experimental spectra shown in figure 15 and 18(b). The resolution of the measurements in figure 18(b) is 0.7 nm. Figure 18(b) was measured at much higher currents, in pulsed mode operation. We see that the theory and the experiment are similar (with reasonable values of the parameters), but that the relative intensities of the peaks are not reproduced. This may be due to the fact that our

model is linear and cannot go above threshold since, as mentioned above, we do not use a rate equation. Another problem is that we assumed a uniform carrier density in the pumped section. This is most probably not true because the carrier injection is not uniform and the field in the cavity is not uniform either. The field is maximum at the phase shifter and decreases exponentially above and below (see [16]). This will introduce a non-uniformity in the carrier distribution that cannot be compensated for by the carrier diffusion because of the layered structure. So, in the regions of low field, we will have more spontaneous emission. Also, the bottom of the mesa, which is a low field region, is much wider than the top (fig. 13(b)). This means that the light emitted on the sides sees a different vertical structure and may alter the emission spectrum.

Notice in figure 18 the slight shift in peak position with increasing carrier density. This is due to the change in the index of refraction of the GaAs layers with the carrier density. In our model, we used [6]:

$$\Delta n = 2.2\times10^{-8}N^{1/3} - 1.6\times10^{-14}N^{2/3} - 9.75\times10^{-22}N \tag{20}$$

where Δn is the index change and N is the carrier density in cm^{-3}. We also incorporated a dependence on temperature [15]:

$$\Delta n = 4\times10^{-4}(T-300) \tag{21}$$

where T is the absolute temperature in Kelvins. We assumed that the change in index of refraction was the same for the GaAs and the GaAlAs layers.

This effect of the temperature on the index of refraction is responsible for the shift in peak positions that we observe in figure 19, which shows the emission spectrum at several temperatures (with the carrier density kept constant). Figure 19(a) shows the theoretical calculations and figure 19(b) shows the experimental result. Once again, the agreement is good, except for the relative peak amplitudes. We notice that when the temperature changes, the relative peak amplitudes change also. This is due in part to the modification of the gain spectrum with temperature, as shown in figure 17(b). This

modification is due to a number of factors, the main ones being the change of the bandgap and that of the density of states with temperature. We see that the wavelength of maximum gain changes and so does the value of that maximum gain. When the mode position coincides with the maximum gain, the peak amplitude is maximum. This occurs around 300K for the peak at 884 nm (at 300K). When we change the temperature, the maximum gain and the mode shift at different rates and, as a result, the peak amplitude decreases.

IX. Conclusions

In this paper, we have developed a way to compute the propagation constants of the modes in a one-dimensional periodic structure over a certain band of frequency, when material dispersion is present. The correct interpretation of the solutions is based on the direction of the power flow. This led us to discover that, for a structure with even symmetry, the backward and forward propagating modes exchange their roles when the gain changes sign in the stop-band. These results were checked in the two layers case by obtaining an exact solution. We then derived the formulas for the reflection and transmission coefficients at the interface between a periodic and a uniform section.

Using these results, we developed a model to compute the emission spectrum of the surface-emitting laser diode (SELD) below threshold. We made several assumptions in this model. The main ones are: (1) The Bloch wave description for the electric field is accurate. (2) The carrier density is uniform in the pumped region. (3) The horizontal cross-section (parallel to the layers) is constant from the top to the bottom. We think that the first assumption is a good approximation, but that the second and third ones are partially responsible for the discrepancies between the theory and the experimental results. Our confidence in the first assumption comes from the good agreement between theory and experiment for the reflectivity of the layered structure (section VI).

As mentioned in section VIII and in the previous paragraph, the assumption of a uniform carrier density is probably not a good one. A variation in carrier density will result in a longitudinal gain non-uniformity, which may change the threshold gain for the modes and hence explain the difference in the relative peak amplitudes between theory and experiment. The fact that the cavity is really trapezoidal (and not rectangular, as implied by the third assumption) may give a significant contribution to spontaneous emission and modify the spectrum, since the light emitted on the sides sees a different vertical structure (see fig. 13).

In conclusion, we can say that our model is sufficient to explain a lot of the observed characteristics of the spectrum. To get a better agreement, we need to extend its validity above threshold. To do that, we need to incorporate rate equations for the carrier density. The next step would be to take into account the longitudinal non-uniformity of the carrier density, but that is much more difficult and can probably not be done using the theory developed in this paper. One way to do it would be to use a transfer matrix for each period (see for example [13]) and solve self-consistently.

On the experimental side, we are now working on several improvements, such as using reactive ion-beam etching to get vertical side-walls to the cavity, which would avoid the problems due to a trapezoidal cavity. We are considering replacing the zinc diffusion, which is difficult to control, by a two steps LPE process. We grow first n-type GaAlAs on one side of the mesa, then p-type GaAlAs on the other side, so that we still get a transverse p-n junction. We are also working on distributed Bragg reflector (DBR)-type structures, where we have a relatively long uniform active region (3-5 μm) between a bottom unpumped multilayer and a top dielectric multilayer.

Acknowledgments

The authors acknowledge contributions from Jane J. Yang of Space and Technology group, TRW, from Lillian Z. Gacusan and Larry Dries of the Lockheed Missiles & Space Company. We would also like to thank Professor John R. Whinnery for his continuous support and Mike Werner, Daryoosh Vakshoori and Myra Boenke for their suggestions and stimulating discussions.

This work is supported by Lockheed Missiles & Space Company, by a grant from the California State Micro program and in part by the Office of Naval Research (ONR).

Appendix A

In this appendix, we derive the exact expression of the average over one period of the time averaged Poynting vector. We start with an electric field of the form:

$$E_y=\left[c_1e^{(g-j\beta)z}+c_2e^{-(g-j\beta)z}\right]e^{j\omega t} \tag{A.1}$$

Using Maxwell's equations, this gives:

$$H_x=-\frac{j}{\omega\mu_0}(g-j\beta)\left[c_1e^{(g-j\beta)z}-c_2e^{-(g-j\beta)z}\right]e^{j\omega t} \tag{A.2}$$

The time averaged Poynting vector is:

$$\vec{S}=\frac{1}{2}\text{Re}(\vec{E}\times\vec{H}^*)=-\frac{1}{2}\text{Re}(E_yH_x^*)\vec{e}_z \tag{A.3}$$

Which gives us:

$$S_z=\frac{\beta}{2\omega\mu_0}\left[|c_1|^2e^{2gz}-|c_2|^2e^{-2gz}\right]+\frac{g}{\omega\mu_0}\text{Im}\left[c_1^*c_2e^{j2\beta z}\right] \tag{A.4}$$

Now, for $E_y=A(z)e^{\Gamma z}$, where A(z) is given by (27), the average of S_z over one spatial period is given by:

$$\begin{aligned}
\langle S_z\rangle &= \frac{1}{\Lambda}\int_{-z_1}^{z_2} S_z\,dz \\
&= \frac{|A_1|^2}{\omega\mu_0\Lambda}\left\{\frac{\beta_1}{2}\left[\frac{1-e^{-2g_1z_1}}{2g_1}+|s_1|^2\frac{e^{2g_1z_1}-1}{2g_1}\right]\right. \\
&\quad+\frac{\beta_2}{2}\left[|s_3|^2\frac{e^{2g_2z_2}-1}{2g_2}+|s_4|^2\frac{1-e^{-2g_2z_2}}{2g_2}\right] \\
&\quad\left.+\text{Im}\left[g_1s_1\frac{1-e^{-j2\beta_1z_1}}{j2\beta_1}+g_2s_3^*s_4\frac{e^{j2\beta_2z_2}-1}{j2\beta_2}\right]\right\}
\end{aligned} \tag{A.5}$$

Appendix B

This appendix gives the expressions for the reflection and transmission coefficients and for the propagation factors used to compute the reflectivity, in (44), and the emission spectrum, in (46)-(51). With $L_1=z_2-z_1$ and $L_3=z'_4-z'_3$ (fig. 11 and 16), we have:

$$R_1=\frac{s_{f1}-r}{1-r\,s_{f1}} \qquad T_1=\frac{1-r}{1-r\,s_{f1}}[1+s_{f1}]$$

$$R_2=\frac{r-s_{b1}}{1-r\,s_{f1}}\left[\frac{1+s_{f1}}{1+s_{b1}}\right] \qquad T_2=(1+r)\frac{1-s_{f1}s_{b1}}{1-r\,s_{f1}}\left[\frac{1}{1+s_{b1}}\right]$$

$$R_3=\frac{P_u^2 s_{f3}-s_{f2}}{1-P_u^2 s_{b2}s_{f3}}\left[\frac{1+s_{b2}}{1+s_{f2}}\right] \qquad T_3=\frac{P_u(1-s_{f2}s_{b2})}{1-P_u^2 s_{b2}s_{f3}}\left[\frac{1+s_{f3}}{1+s_{f2}}\right]$$

$$R_4=\frac{P_u^2 s_{b2}-s_{b3}}{1-P_u^2 s_{b2}s_{f3}}\left[\frac{1+s_{f3}}{1+s_{b3}}\right] \qquad T_4=\frac{P_u(1-s_{f3}s_{b3})}{1-P_u^2 s_{b2}s_{f3}}\left[\frac{1+s_{b2}}{1+s_{b3}}\right] \qquad \text{(B.1)}$$

where

$$P_u=\exp((g_2-j\,\beta_2)L_2) \quad \text{and} \quad r=\frac{K_B-k_0}{K_B+k_0}$$

$$P_1=D_f=\left[\frac{1+s_{f2}}{1+s_{f1}}\right]e^{\Gamma L_1} \qquad P_2=D_b=\left[\frac{1+s_{b1}}{1+s_{b2}}\right]e^{\Gamma L_1}$$

$$P_3=\left[\frac{1+s_{f4}}{1+s_{f3}}\right]e^{\Gamma L_3} \qquad P_4=\left[\frac{1+s_{b3}}{1+s_{b4}}\right]e^{\Gamma L_4} \qquad \text{(B.2)}$$

The coefficients s_f and s_b are defined in (34). The numerical index indicates at which position z_i they are computed (and $k_0=2\pi/\lambda$).

For the reflectivity calculation (44), we have (fig. 11):

$$R_5=-s_{f4}\left[\frac{1+s_{b4}}{1+s_{f4}}\right] \qquad T_5=(1-s_{f4}s_{b4})\left[\frac{1}{1+s_{f4}}\right] \qquad \text{(B.3)}$$

Notice that for the emission spectrum calculation, L_3 is different from the L_3 in the reflectivity calculation. For the spectrum (46)-(51), we get (fig. 16):

$$R_5=R_6+\frac{T_6T_7P_5P_6R_8}{1-R_7R_8P_5P_6} \tag{B.4}$$

where R_5 is an effective reflection coefficient, for everything to the left of the L_3/L_4 interface in figure 16. And we use (with $L_4=z'_5-z'_4$):

$$R_6=\frac{s^u_{f4}-s_{f4}}{1-s^u_{f4}s_{b4}}\left[\frac{1+s_{b4}}{1+s_{f4}}\right] \qquad T_6=\frac{1-s_{f4}s_{b4}}{1-s^u_{f4}s_{b4}}\left[\frac{1+s^u_{f4}}{1+s_{f4}}\right]$$

$$R_7=\frac{s_{b4}-s^u_{b4}}{1-s^u_{f4}s_{b4}}\left[\frac{1+s^u_{f4}}{1+s^u_{b4}}\right] \qquad T_7=\frac{1-s^u_{f4}s^u_{b4}}{1-s^u_{f4}s_{b4}}\left[\frac{1+s_{b4}}{1+s^u_{b4}}\right]$$

$$R_8=-s^u_{f5}\left[\frac{1+s^u_{b5}}{1+s^u_{f5}}\right] \qquad P_5=\left[\frac{1+s^u_{f5}}{1+s^u_{f4}}\right]e^{\Gamma_u L_4} \qquad P_6=\left[\frac{1+s^u_{b4}}{1+s^u_{b5}}\right]e^{\Gamma_u L_4} \tag{B.5}$$

The superscript u for s indicates here that it is the s of the unpumped section (L_4) that has to be used.

References

[1] C. Elachi, *"Waves in active and passive periodic structures: A review"*, Proc. of the IEEE, vol 64 (12), pp 1666-1698 (1976).

[2] M. Ogura *et al*, *"Surface-emitting laser diode with vertical GaAs/GaAlAs quarter-wavelength multilayers and lateral buried heterostructure"*, Appl. Phys. Lett., 51(21), pp 1655-1657, 23 November 1987.

[3] Wei Hsin *et al*, *"GaAs/GaAlAs surface emitting laser diode with vertical distributed feedback cavity and transverse junction burried heterostructure"*, IEDM 1987 Technical Digest, paper 34.3, Washington DC (1987).

[4] F. Koyama, K. Tomomatsu and K. Iga, *"GaAs surface emitting lasers with circular buried heterostructure grown by metalorganic chemical vapor deposition and two-dimensional laser array"*, Appl. Phys. Lett., 52(7), pp 528-531, 15 February 1988. See also the references therein.

[5] S. Wang, *"Principles of distributed feedback and distributed Bragg-reflector lasers"*, IEEE J. Quantum Elec., QE-10 (4), pp 413-427 (1974).

[6] S. Wang, *"Integratable active and passive optical devices"*, in: Semicond. and Semimetals, vol 22, part E (W.T.Tsang editor), 1985, see pp 52-64

[7] A. Yariv, *"Quantum Electronics (2nd Edition)"*, Wiley, New York, 1975.

[8] S. Wang, *"Thin-film Bragg lasers for integrated optics"*, Wave Electronics, vol 1, pp 31-59 (1974-1975).

[9] A. Yariv and A. Grover, *"Equivalence of the coupled-mode and Floquet-Bloch formalism in periodic optical waveguides"*, Appl. Phys. Lett.,vol 26, pp 537-539 (1975).

[10] H. Soda and H. Imai, *"Analysis of the Spectrum Behavior Below the Threshold in DFB Lasers"*, IEEE J. Quantum Elec., QE-22 (5), pp 637-641 (1986).

[11] L. Brillouin, *"Wave propagation in periodic structures"*, Mc Graw-Hill, New-York, 1946.

[12] Jean-Pierre Weber, unpublished.

[13] G. Bjork and O.Nilsson, *"A new exact and efficient numerical matrix theory of complicated laser structures: Properties of asymmetric phase-shifted DFB lasers"*, J. Lightwave Techn., LT-5 (1), pp 140-146, January 1987.

[14] A. Yariv and P. Yeh, *"Optical waves in crystals"*, Wiley, New York, 1984.

[15] H.C. Casey and M.B. Panish, *"Heterostructure Lasers"*, Part A, Academic, New York (1978).

[16] H.A. Haus, *"Waves and fields in optoelectronics"*, Prentice-Hall, Englewood Cliffs, N.J., 1984.

[17] Jean-Pierre Weber, unpublished.

Figure captions

Figure 1: Examples of periodic structure that give a one-dimensional wave equation: (a) waveguides, (b) multilayers.

Figure 2: Definition of the parameters for the two-layers structure.

Figure 3: Intensity gain in GaAs, as a function of free space wavelength for three different carrier densities: (1) $N=0.2\times10^{18}\ cm^{-3}$, (2) $N=1.0\times10^{18}\ cm^{-3}$, (3) $N=2.0\times10^{18}\ cm^{-3}$.

Figure 4: G and δ_{eff} for the structure of table 1: (a) without gain or loss, (b) with 2000 cm^{-1} average gain, but neglecting gain periodicity, (c) as in b, but with gain periodicity (see text).

Figure 5: G and δ_{eff} for the structure of table 1 and the intensity gains of figure 3, corresponding to three different carrier densities: (a) $N=0.2\times10^{18}\ cm^{-3}$, (b) $N=1.0\times10^{18}\ cm^{-3}$, (c) $N=2.0\times10^{18}\ cm^{-3}$.

Figure 6: $|s|$ as a function of wavelength for the two solutions of eq. (13), at three diffrent carrier densities (Fig. 3): (a) $N=0.2\times10^{18}\ cm^{-3}$, (b) $N=1.0\times10^{18}\ cm^{-3}$, (c) $N=2.0\times10^{18}\ cm^{-3}$.

Figure 7: Re(s) and Im(s) as functions of wavelength, at three different carrier densities (Fig. 3): (a) $N=0.2\times10^{18}\ cm^{-3}$, (b) $N=1.0\times10^{18}\ cm^{-3}$, (c) $N=2.0\times10^{18}\ cm^{-3}$.

Figure 8: Definition of the transmission and reflection coefficients at a periodic/uniform regions interface (equation (39)).

Figure 9: Definition of the transmission and reflection coefficients at a phase shifter (equation (43)).

Figure 10: Model used for reflectivity and emission spectrum calculations. One pair consists of a quater-wavelength layer of GaAs and a quarter-wavelength layer of GaAlAs. Dimensions are given in Table 1.

Figure 11: Definition of the coefficients for the reflectivity calculation (44).

Figure 12: (a) Result of the reflectivity calculation, with a center wavelength of λ_0= 893 nm. (b) Comparaison of experiment with best theoretical result (see text).

Figure 13: (a) Structure of the surface-emitting laser diode (SELD). (b) Scanning electron microscope picture of a SELD.

Figure 14: L-I characteristic of a SELD at room temperature, CW operation.

Figure 15: Emission spectrum of a SELD at different drive currents, room temperature, CW operation.

Figure 16: Definition of the coefficients for the emission spectrum calculation (equations (46-51).

Figure 17: GaAs intensity gain curves ($N_A=2\times10^{18}$ cm^{-3}): (a) at T=300K, for several carrier densities, (b) at $N=1.0\times10^{18}$ cm^{-3} and several temperatures. These were obtained with the same model as for figure 3.

Figure 18: Emission spectrum for several carrier densities (currents) at 300K: (a) theory (λ_0= 890 nm, phase shifter thickness = 0.4 Λ), (b) experiment (pulsed mode operation).

Figure 19: Emission spectrum for several temperature, at constant carrier density (current): (a) theory (N= 1.0×10^{18} cm^{-3}, same parameters as in figure 18), (b) experiment (I=320 mA, pulsed operation).

Table 1	
λ_0	890 nm
$n(GaAs)=n_1$	3.59
$n(Ga_{0.7}Al_{0.3}As)=n_2$	3.394
$\bar{n}$ (average index)	3.494
z_1	62 nm
z_2	65.6 nm
Λ	127.6 nm
K_B	2.467×10^7 m^{-1}
$\kappa=\beta_1=\beta_{-1}$	4.4×10^5 m^{-1}
	Amplitude gains
g_1	1/2 of fig. 3 or 17
g_2	- 500 m^{-1}

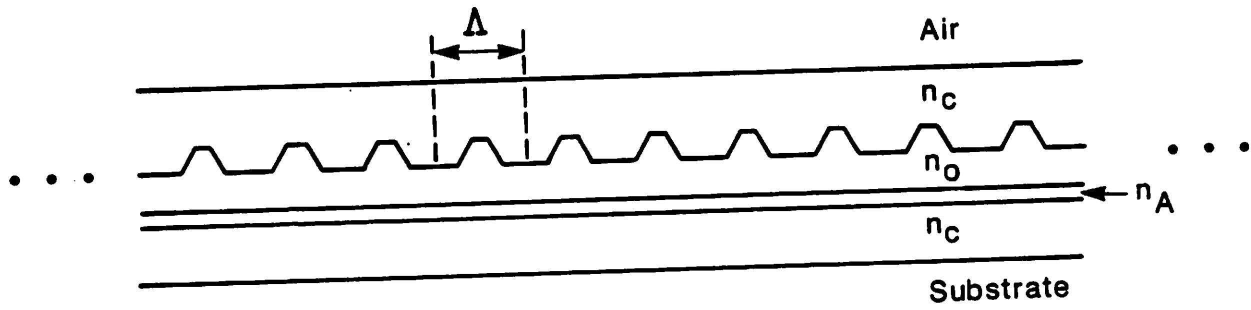

(a)

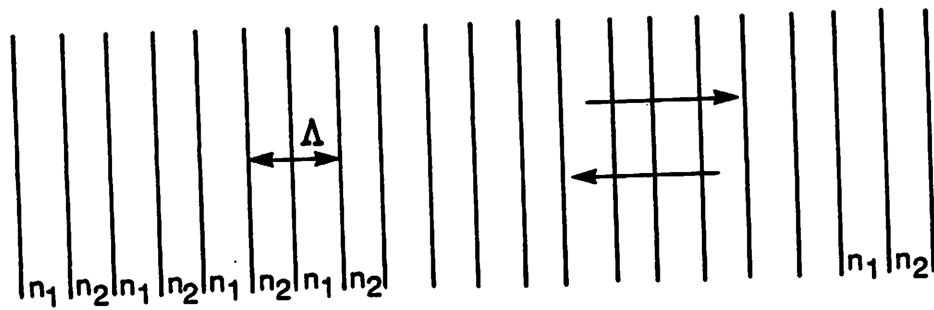

(b)

FIGURE 1

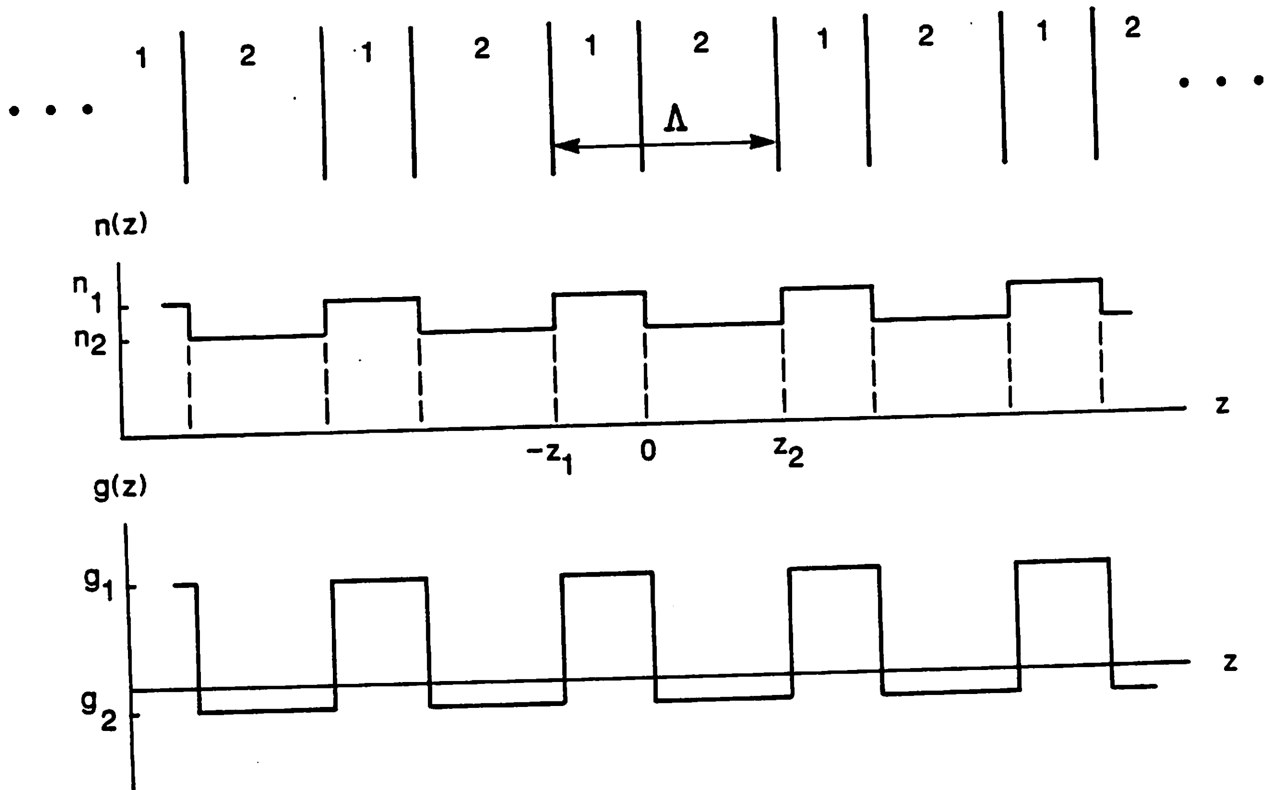

FIGURE 2

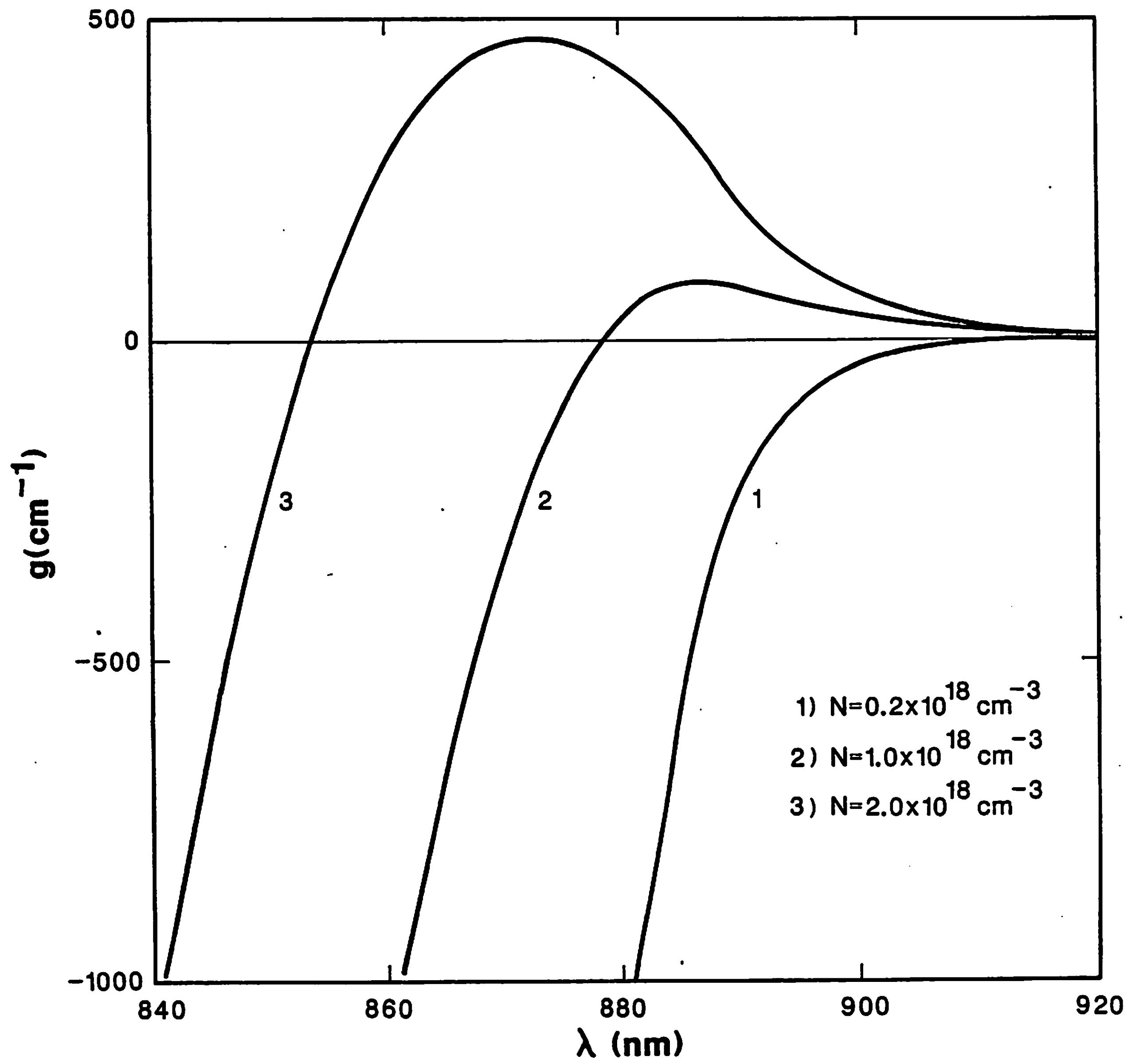

FIGURE 3

(a)

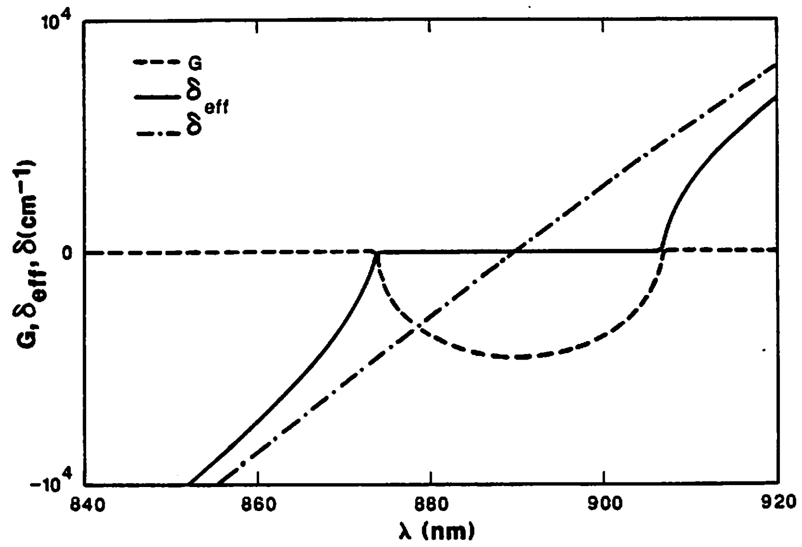

(b)

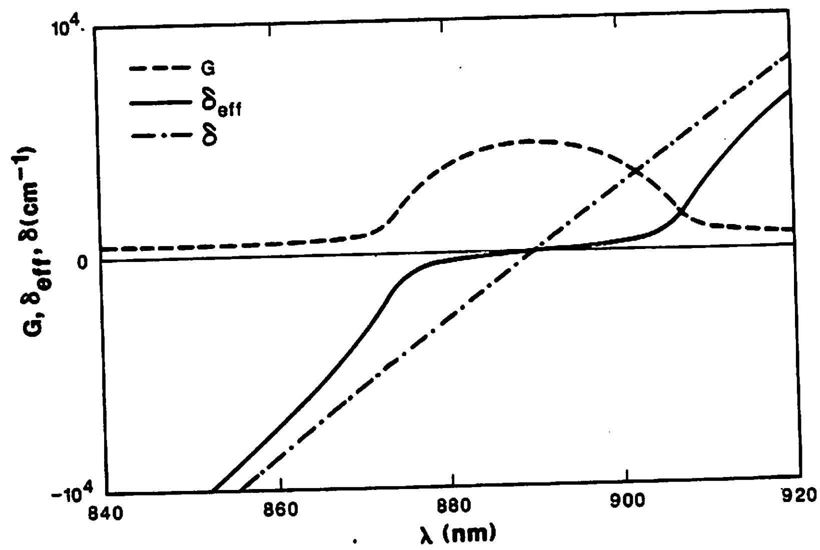

(c)

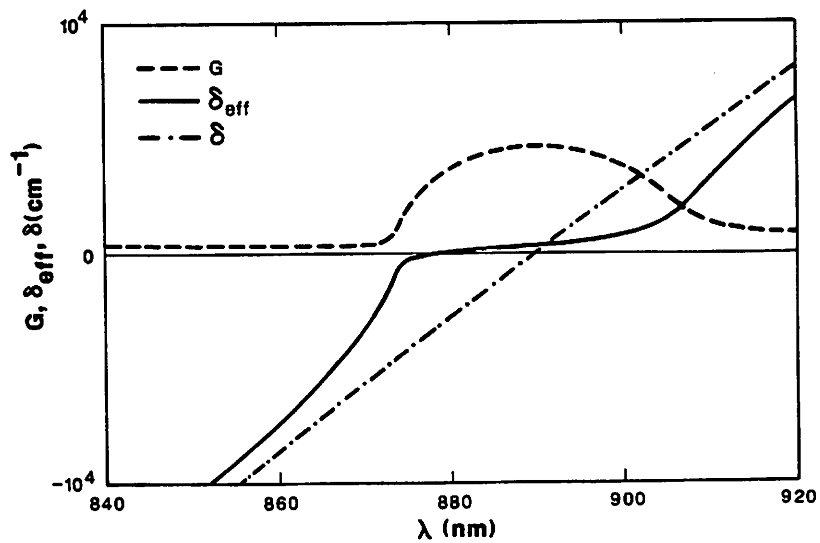

FIGURE 4

(a)

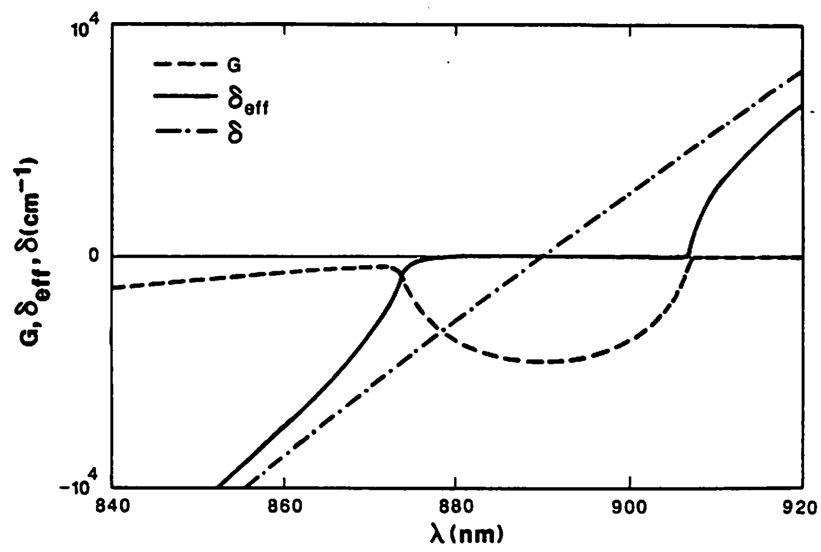

(b)

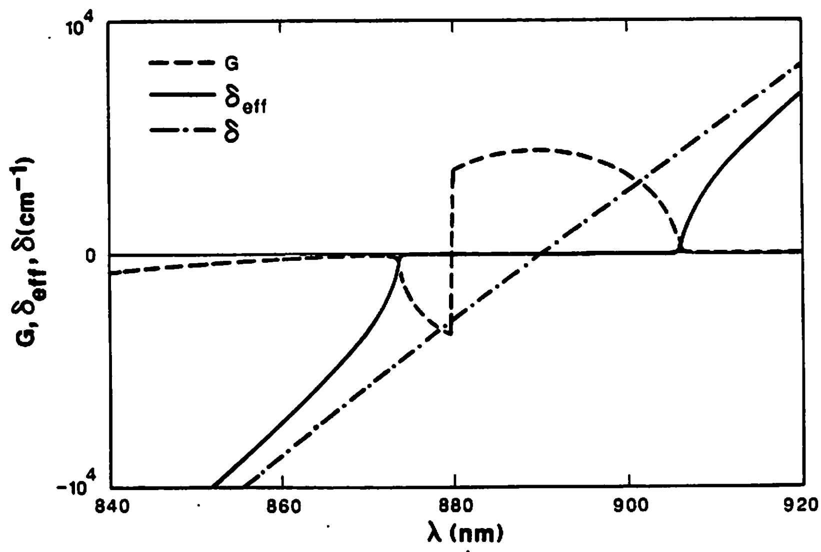

(c)

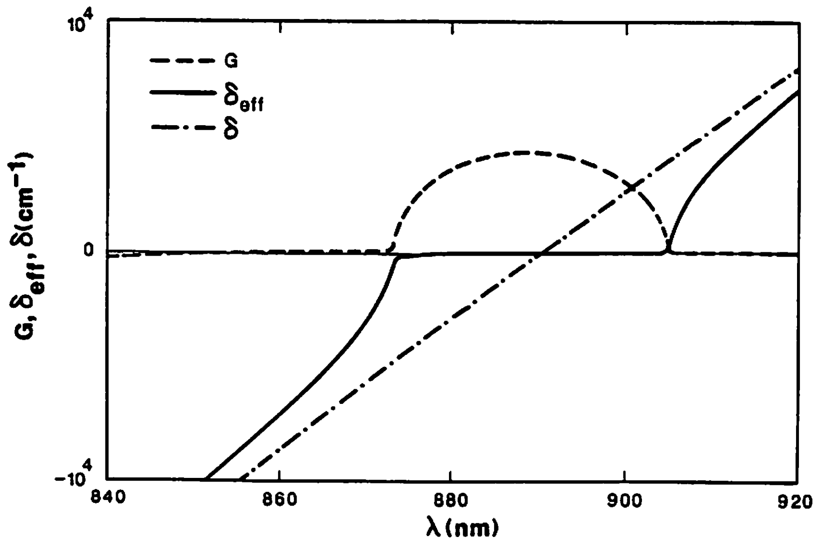

FIGURE 5

(a)

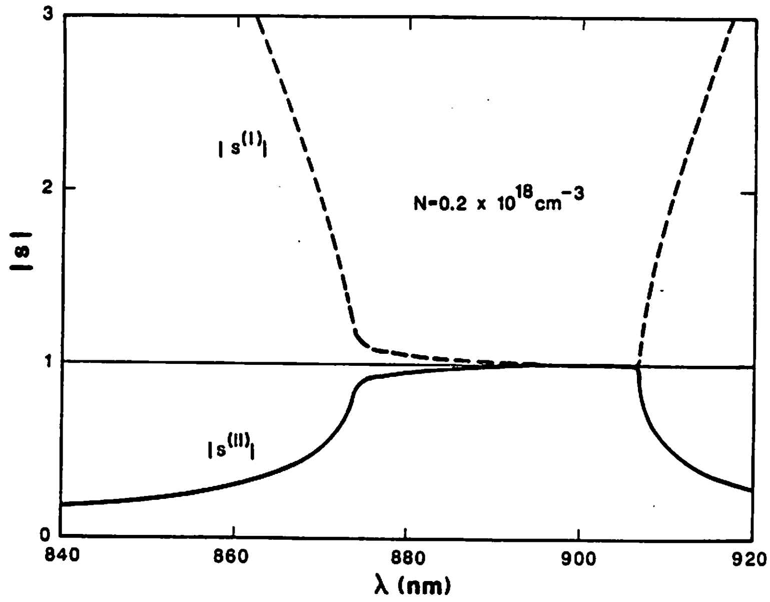

(b)

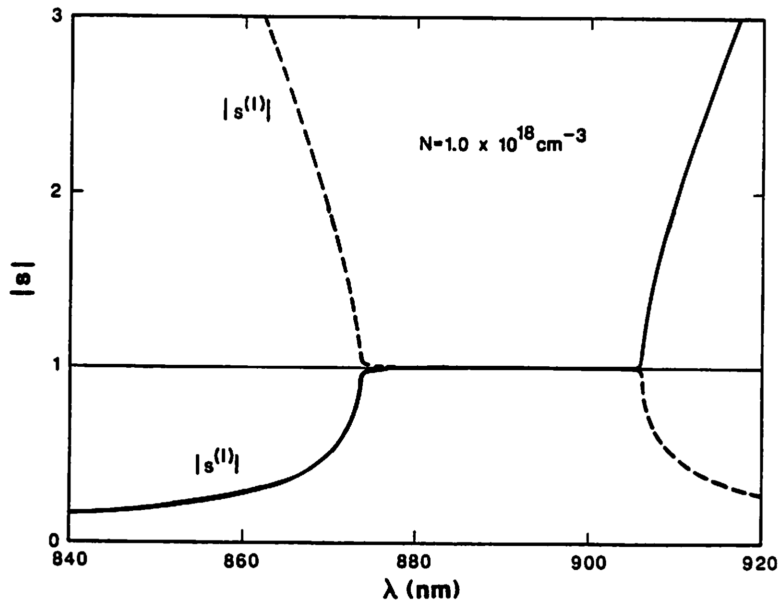

(c)

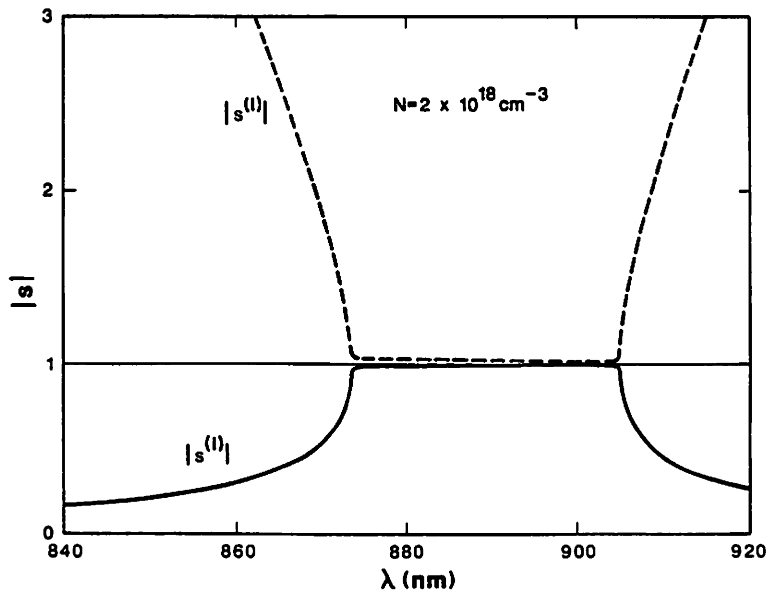

FIGURE 6

(a)

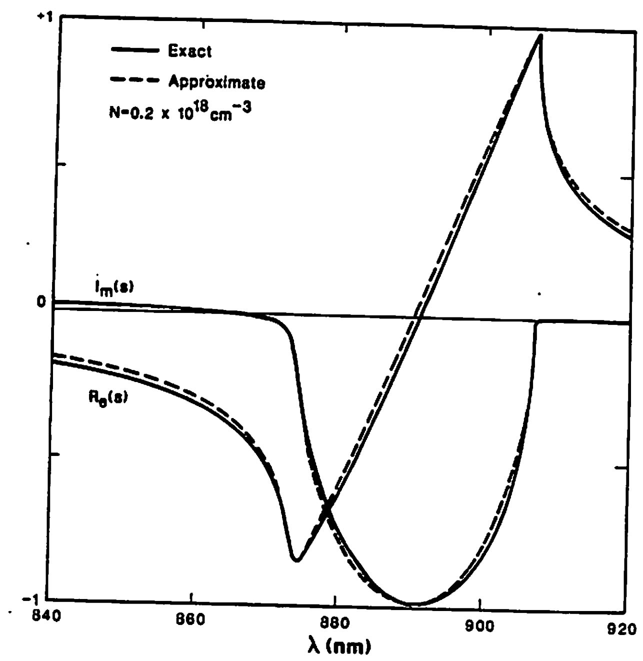

(b)

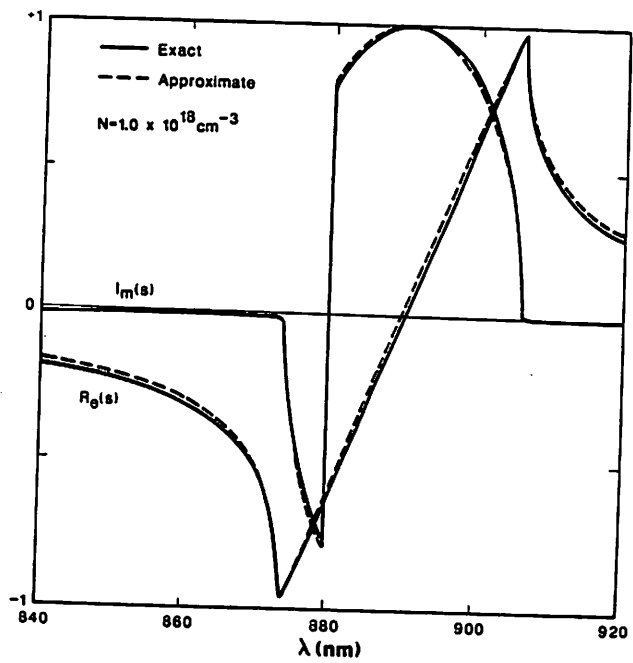

(c)

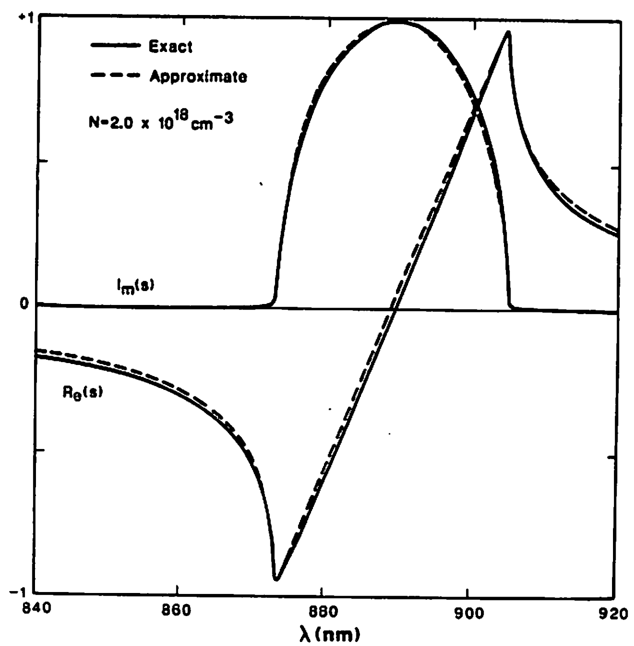

FIGURE 7

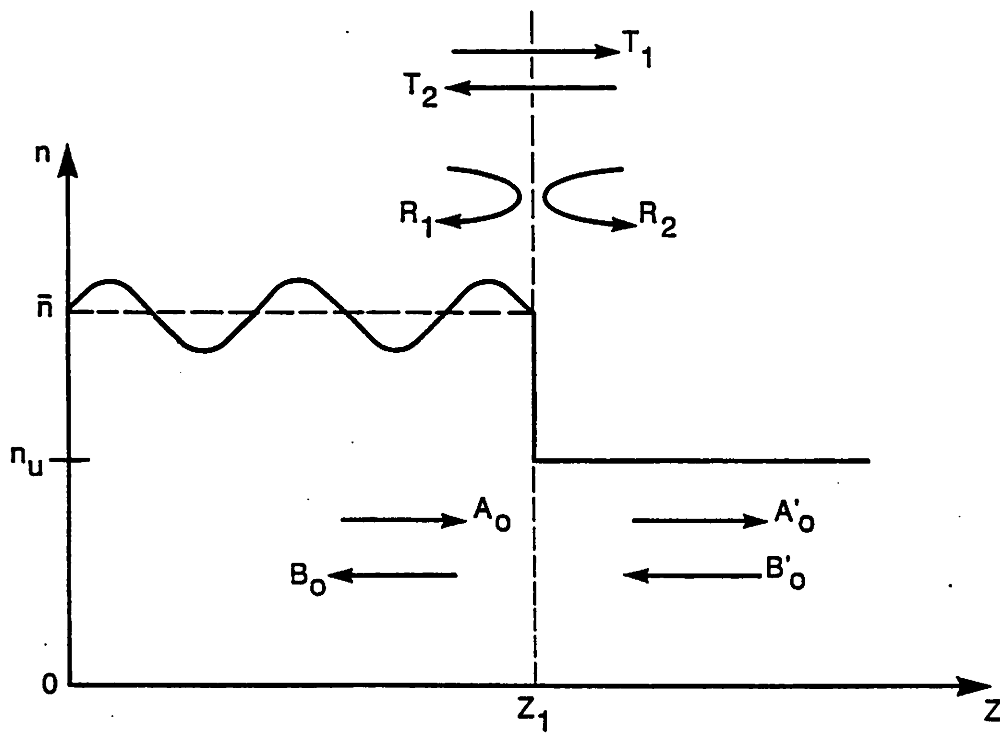

FIGURE 8

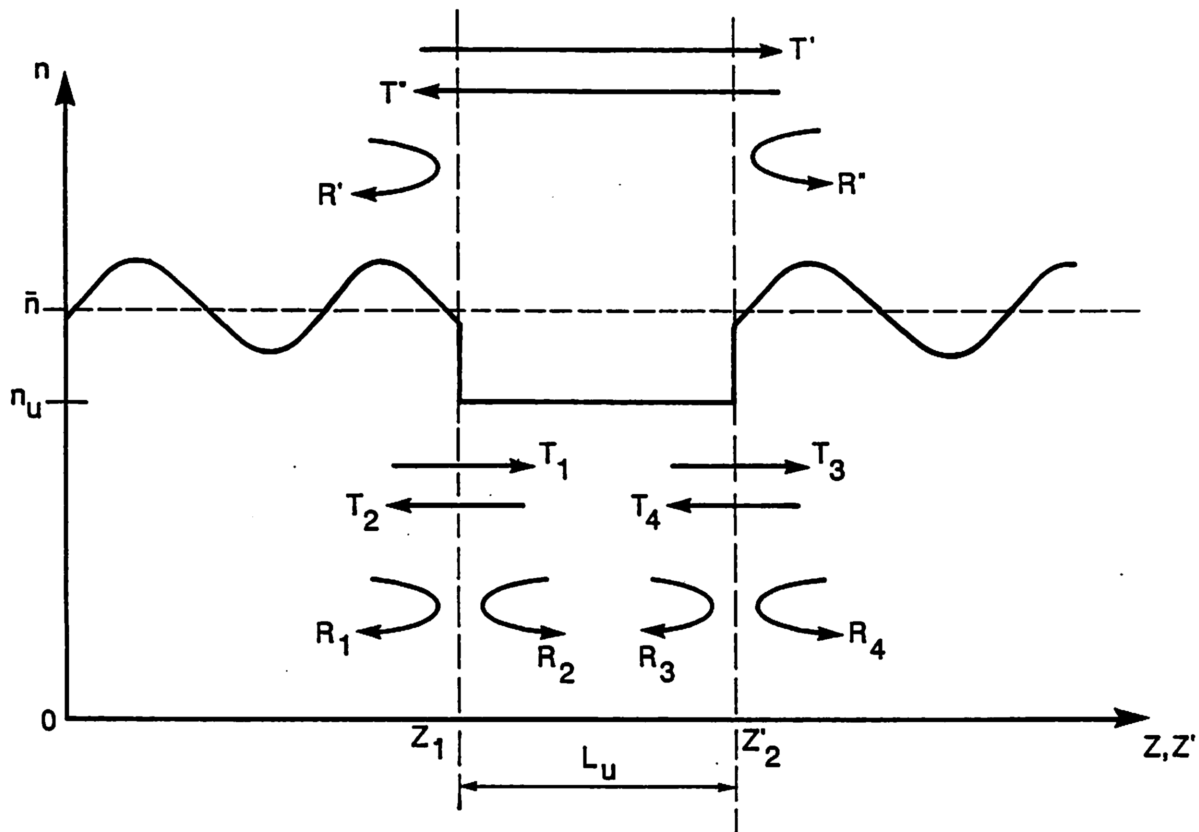

FIGURE 9

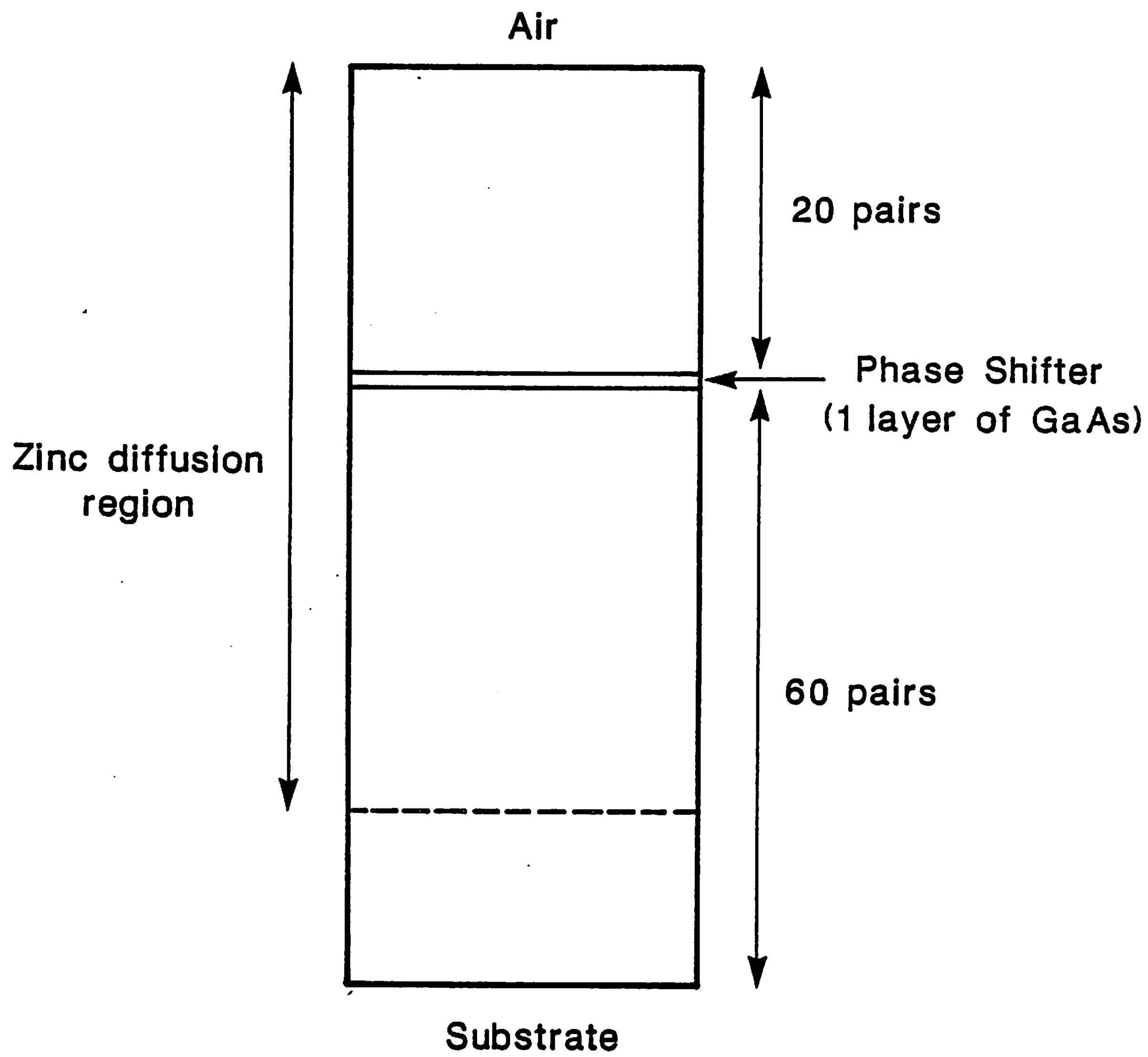

FIGURE 10

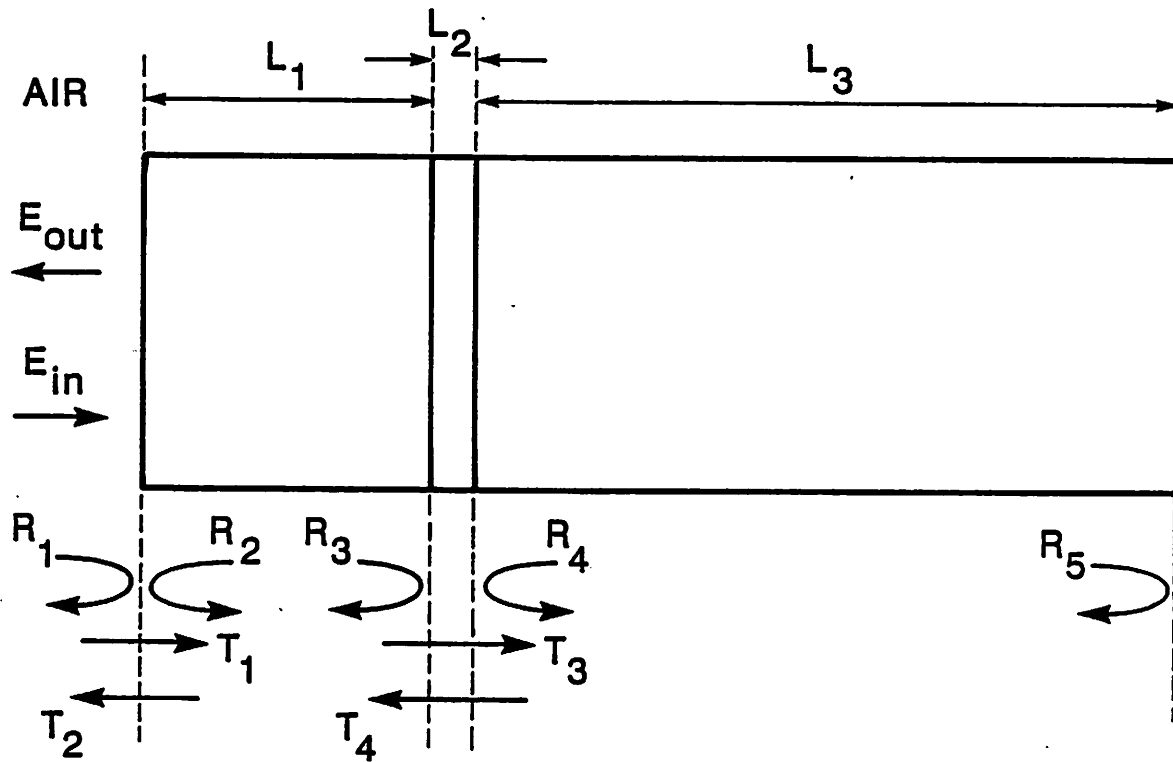

FIGURE 11

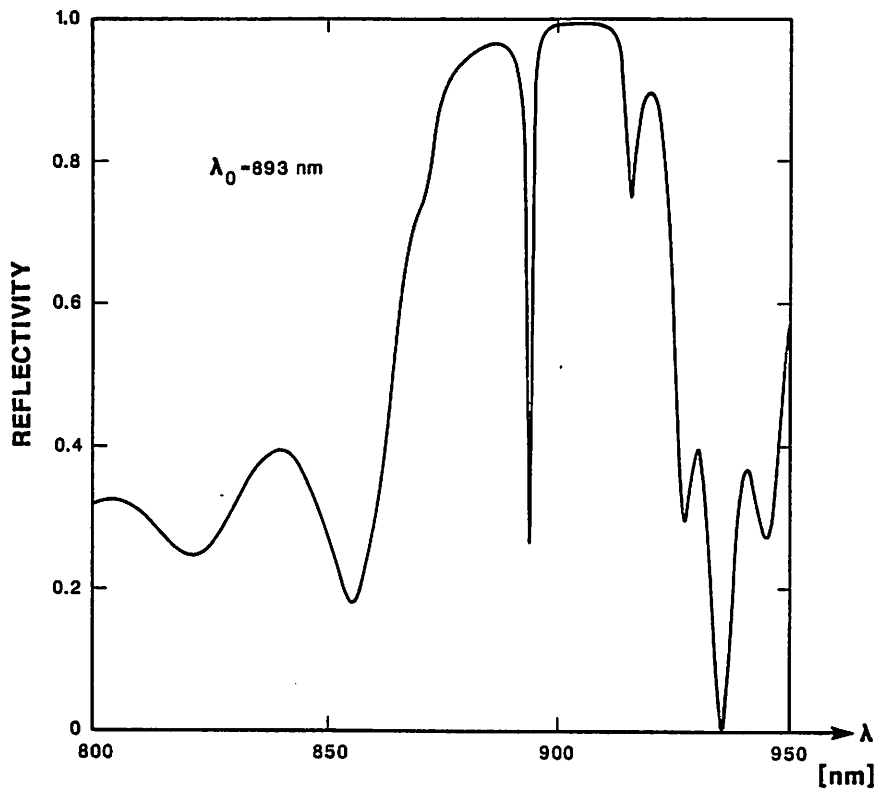

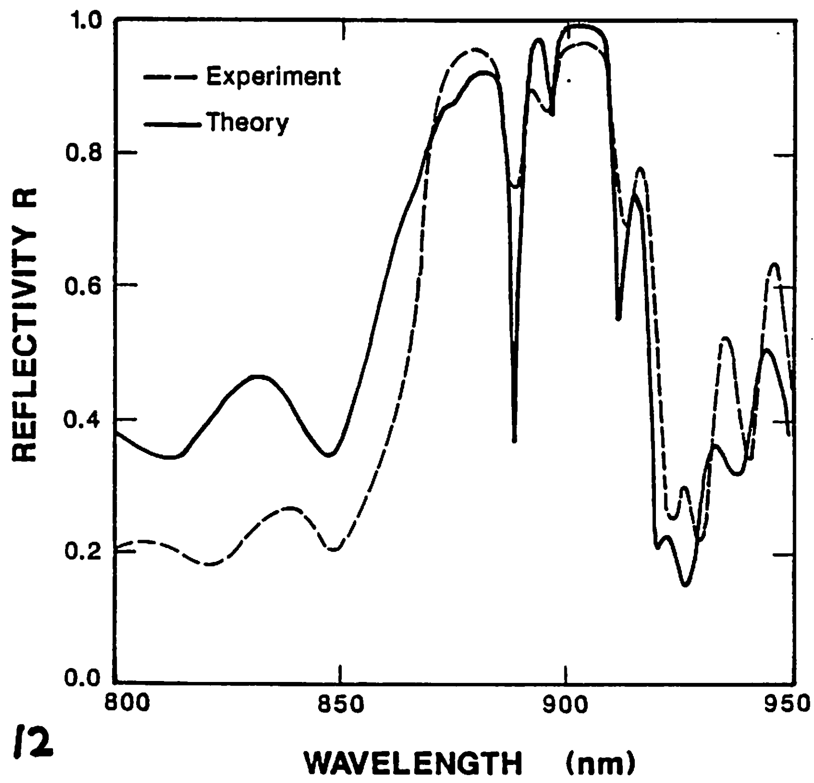

FIGURE 12

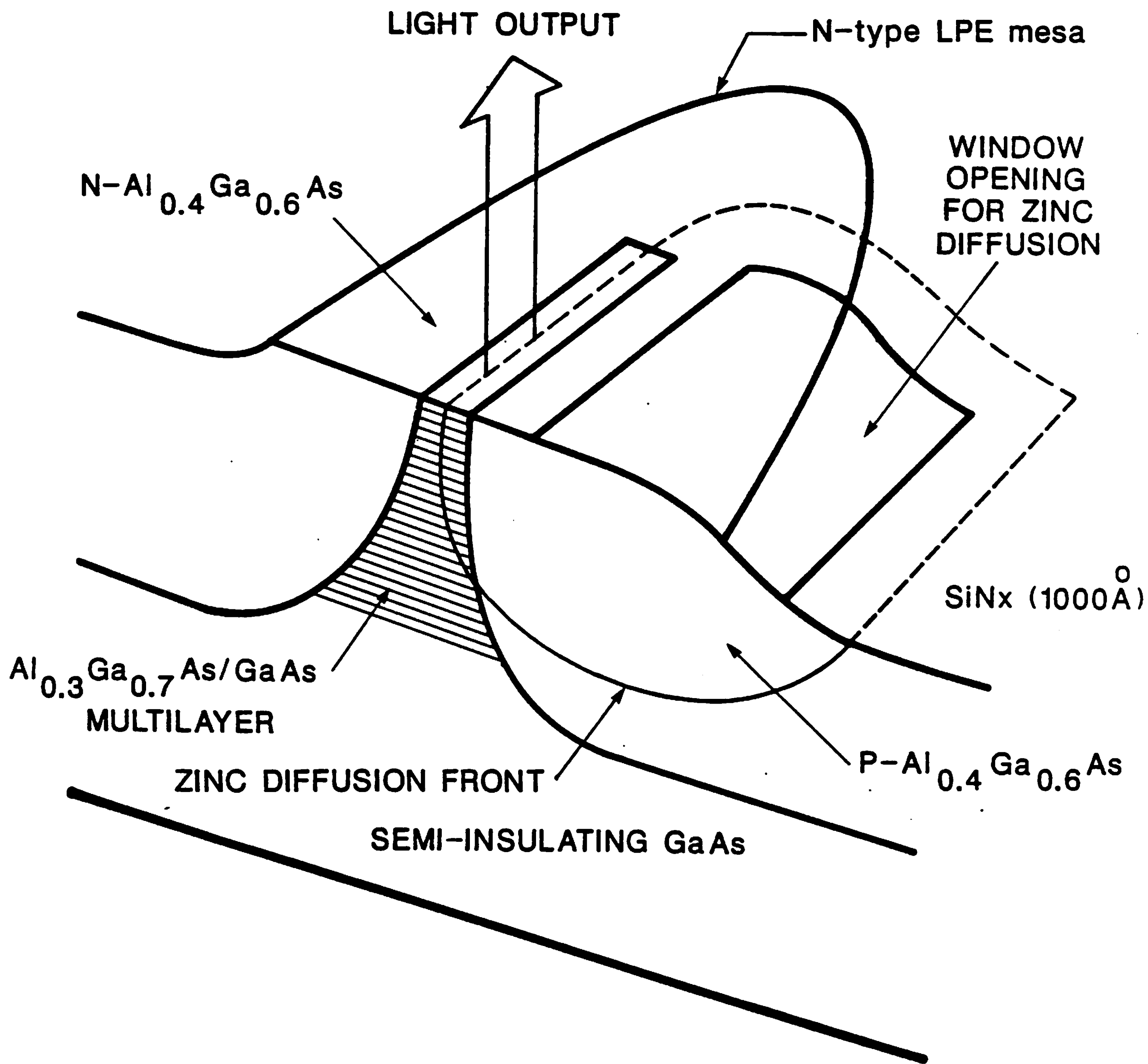

FIGURE 13 (a)

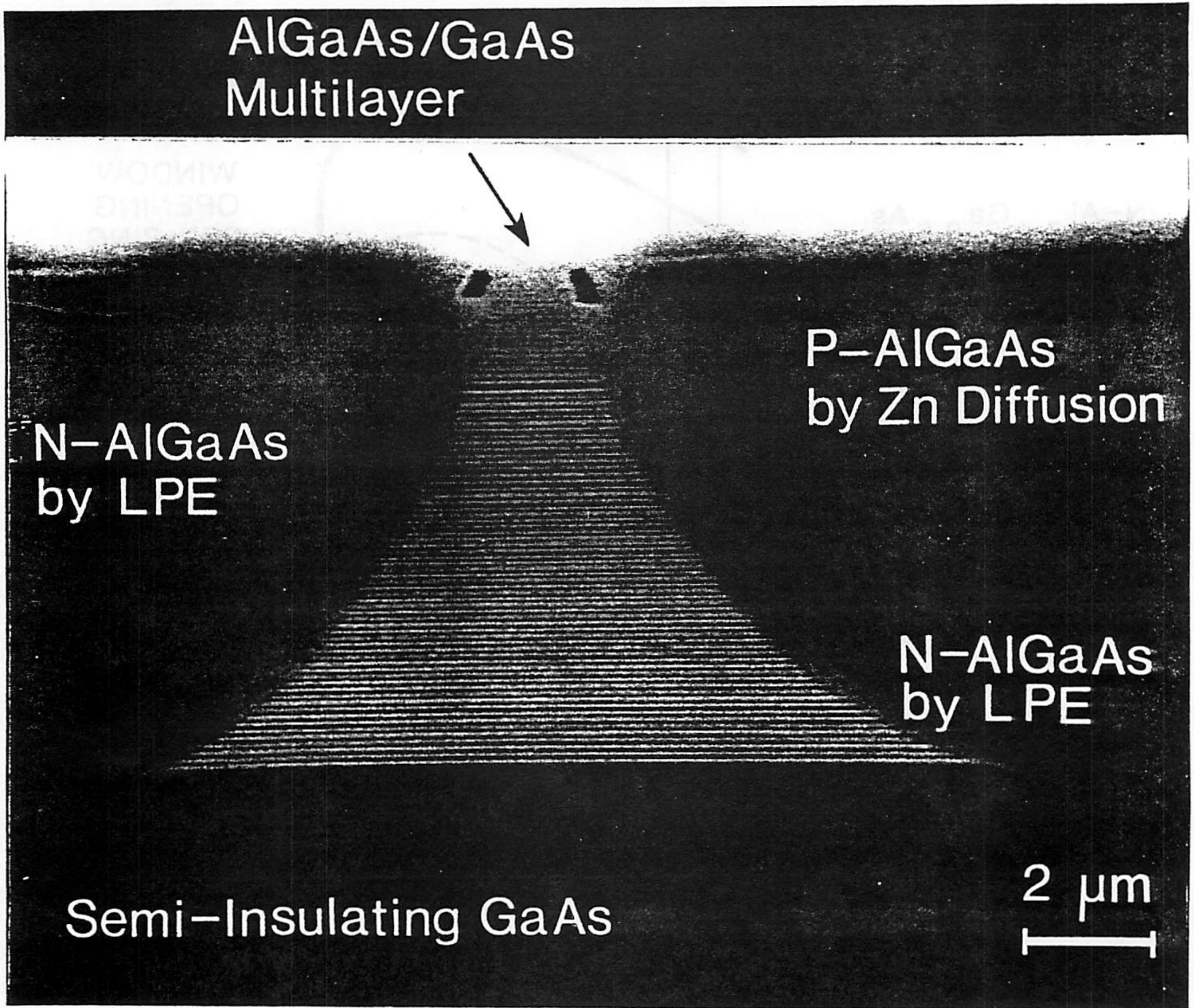

FIGURE 13 (b)

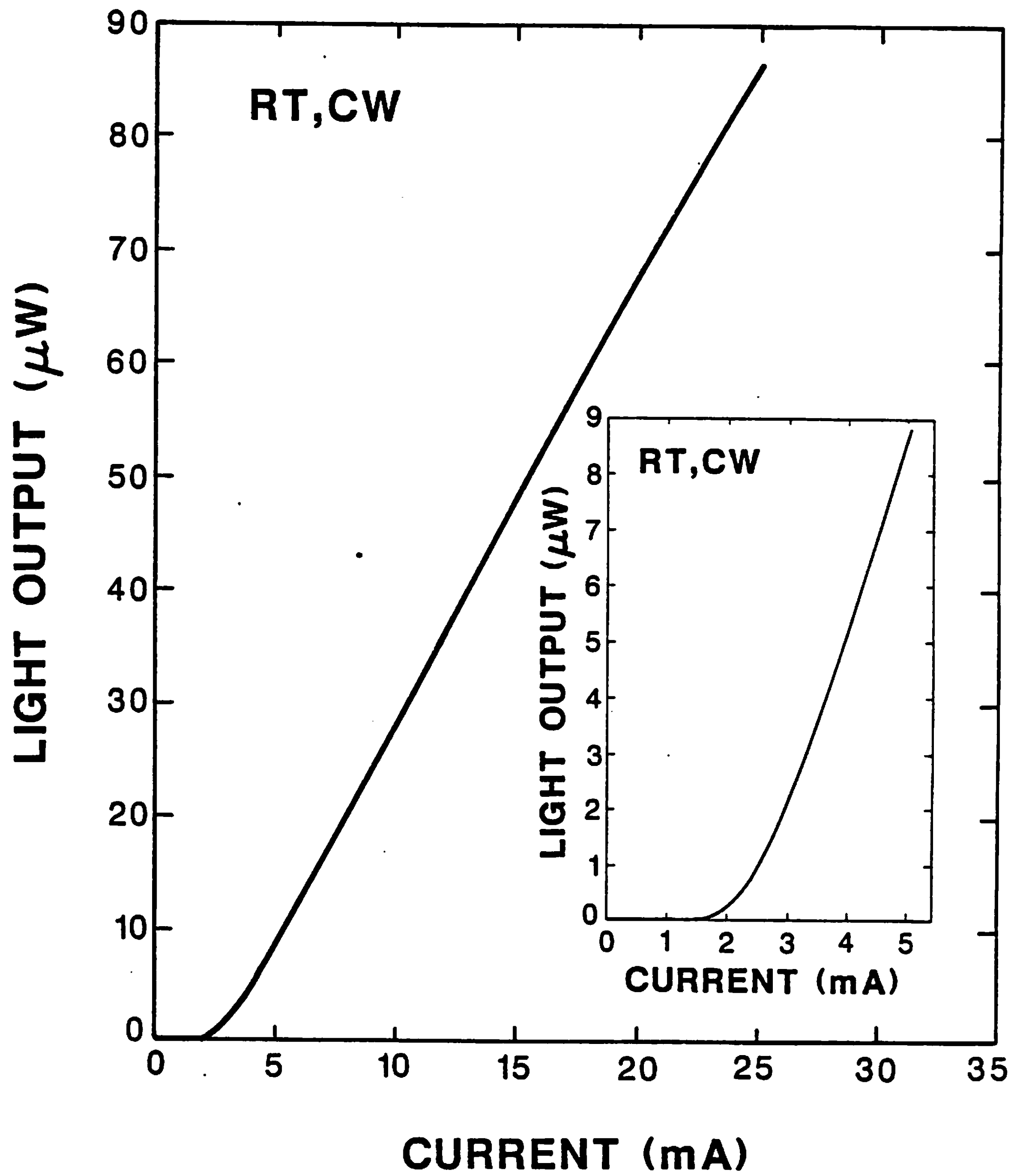

FIGURE 14

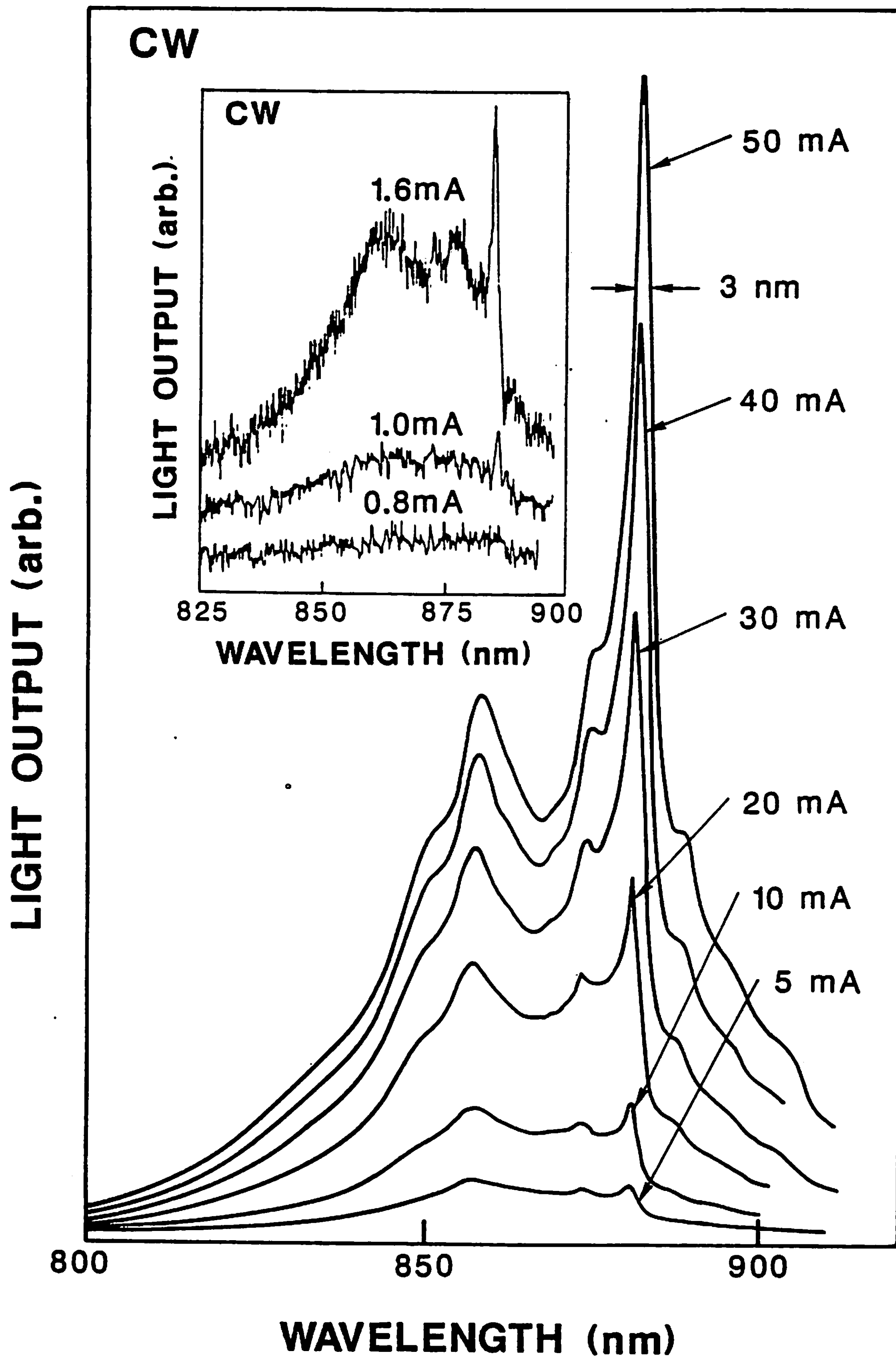

FIGURE 15

(a)

GAIN (cm^{-1})

5×10^2

0

-5×10^2

-10^3

840

920

λ [nm]

T=300K

① N=0.5x10^{18}

② N=1.0x10^{18}

③ N=1.5x10^{18}

③ ② ①

(b)

GAIN (cm^{-1})

10^3

5×10^2

0

-5×10^2

-10^3

840

920

λ [nm]

N=1x10^{18} cm^{-3}

① T=200K

② T=250K

③ T=300K

④ T=350K

① ② ③ ④

FIGURE 17

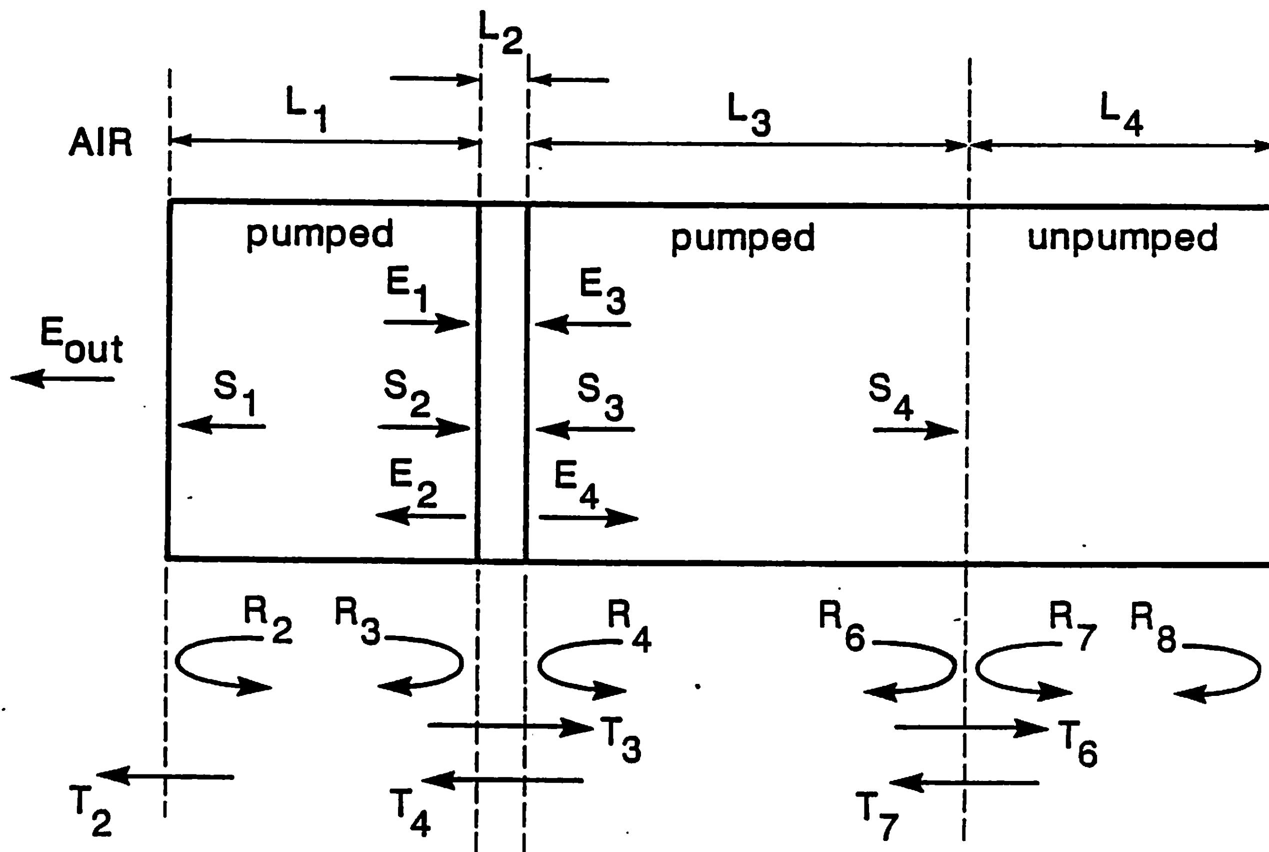

FIGURE 16

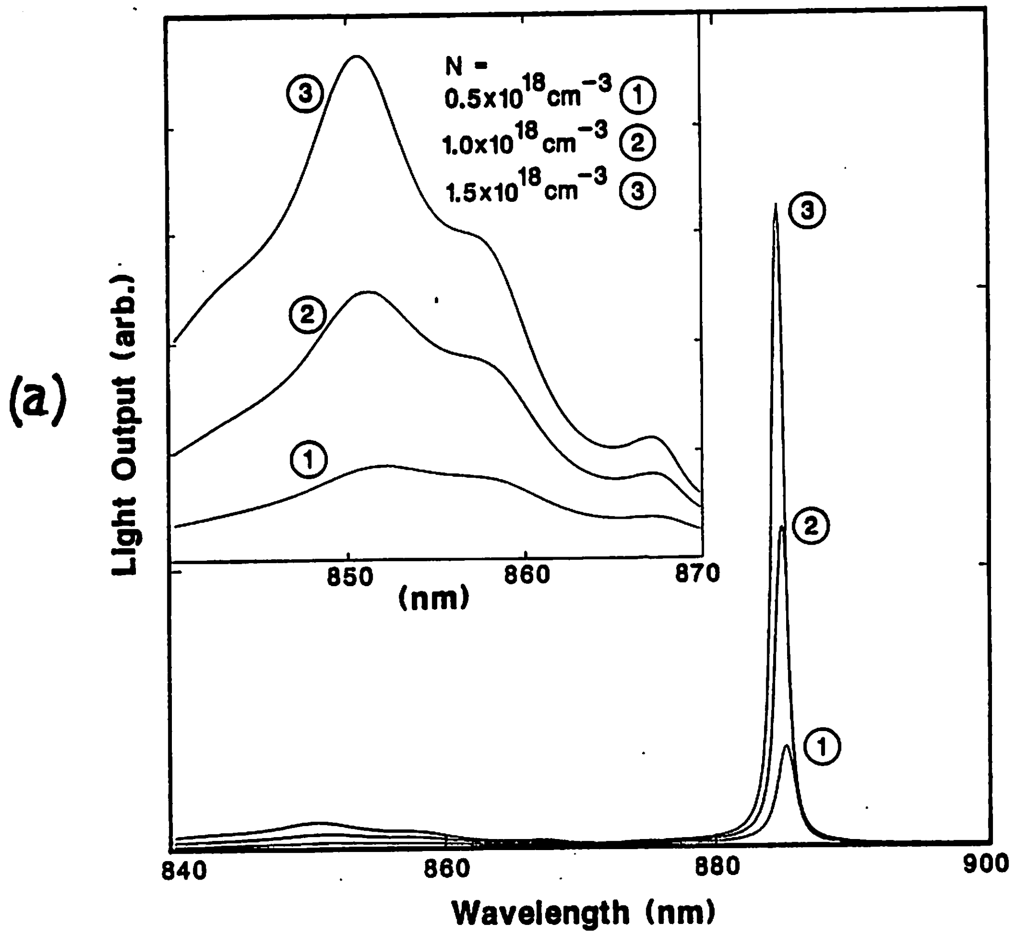

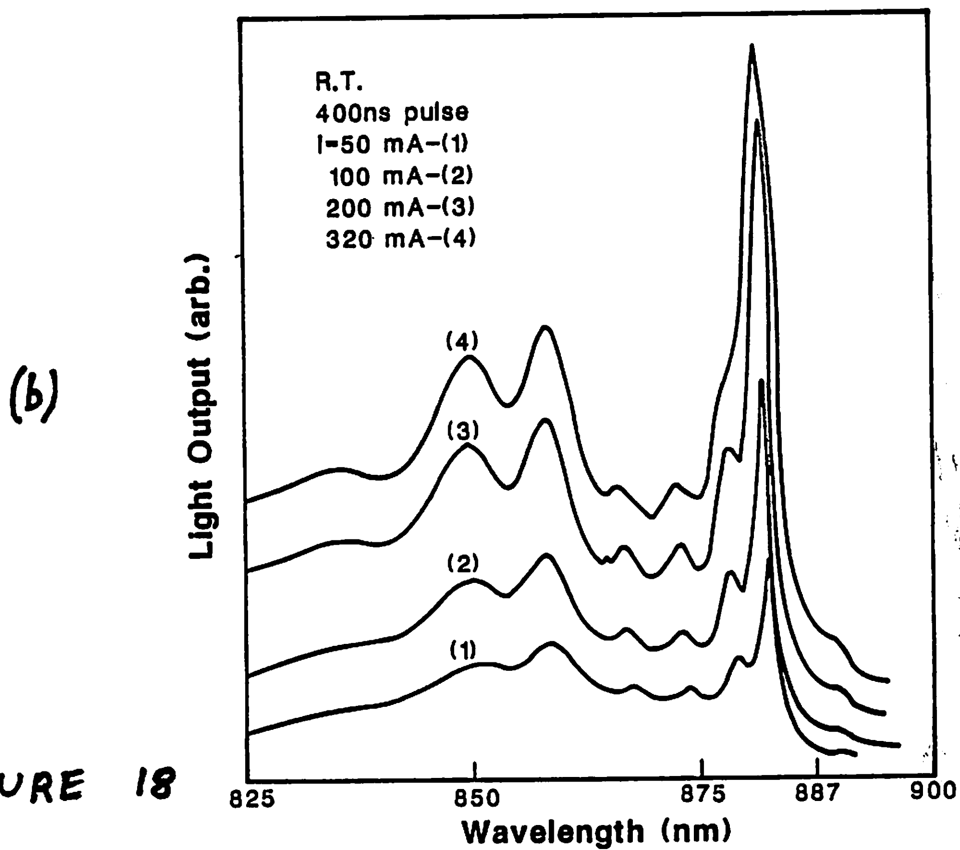

FIGURE 18

(a)

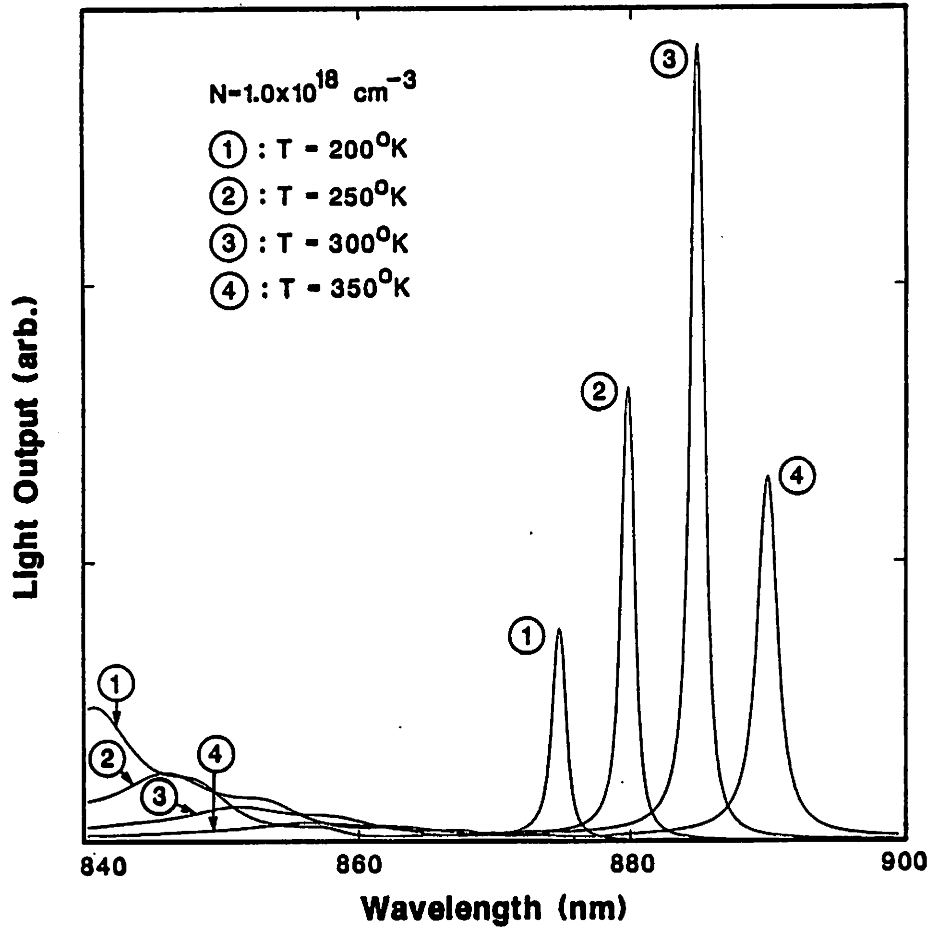

(b)

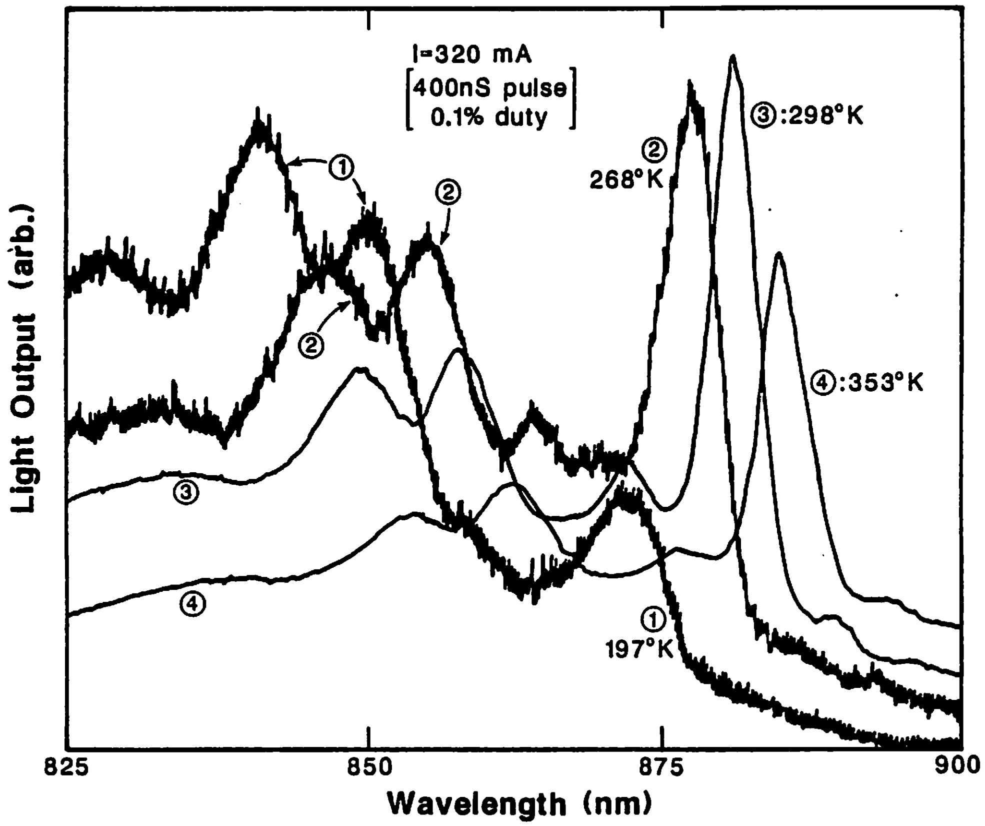

FIGURE 19